Brain, Behavior, & Immunity - Health 28 (2023) 100594

Contents lists available at ScienceDirect

Brain, Behavior, & Immunity - Health

journal homepage: www.editorialmanager.com/bbih/default.aspx

LPS-induced acute neuroinflammation, involving interleukin-1 beta signaling, leads to proteomic, cellular, and network-level changes in the prefrontal cortex of mice

Dániel Mittli [a,b,c], Vanda Tukacs [a,b], Lilla Ravasz [b,d], Éva Csősz [e], Tímea Kozma [d], József Kardos [a], Gábor Juhász [a,b,d,f,1], Katalin Adrienna Kékesi [a,b,c,f,1,*]

[a] ELTE NAP Neuroimmunology Research Group, Department of Biochemistry, Institute of Biology, ELTE Eötvös Loránd University, Budapest, Hungary
[b] Laboratory of Proteomics, Institute of Biology, ELTE Eötvös Loránd University, Budapest, Hungary
[c] Department of Physiology and Neurobiology, Institute of Biology, ELTE Eötvös Loránd University, Budapest, Hungary
[d] CRU Hungary Ltd., Göd, Hungary
[e] Proteomics Core Facility, Department of Biochemistry and Molecular Biology, Faculty of Medicine, University of Debrecen, Debrecen, Hungary
[f] InnoScience Ltd., Mátranovák, Hungary

ARTICLE INFO

Keywords:
Neuroinflammation
Prefrontal cortex
Interleukin-1 beta
Lipopolysaccharide
Patch clamp
Functional connectivity
Proteomics

ABSTRACT

Neuroinflammation induced by peripheral infections leads to various neuropsychiatric symptoms both in humans and laboratory animals, e.g., to the manifestation of sickness behavior that resembles some features of clinical depression. However, in addition to depression-like behavior, there are other symptoms of acute systemic inflammation that can be associated with the impairment of prefrontal cortex (PFC)-regulated cognitive functions. Thus, we investigated the electrophysiological and proteomic alterations of the PFC using brain slices and the lipopolysaccharide (LPS) model of acute peripheral infection in male mice. Based on the gene expression differences of the coreceptor (*Il1rap*) of interleukin-1 beta (IL-1β) between neuron types in our previous single-cell sequencing dataset, we first compared the electrophysiological effects of IL-1β on PFC pyramidal cells and interneurons. We found that pyramidal cells are more responsive to IL-1β, as could be presumed from our transcriptomic data. To examine the possible circuit-level correlates of the cellular changes, frontal electroencephalographic (EEG) activity and fronto-occipital functional connectivity were analyzed in LPS-treated mice and significant changes were found in the fronto-occipital EEG correlation and coherence in the delta and high-gamma frequency bands. The upregulation of the prefrontal IL-1 system (IL-1β and its receptor) after LPS treatment was revealed by immunoassays simultaneously with the observed EEG changes. Furthermore, we investigated the LPS-induced alterations of the synaptic proteome in the PFC using 2-D differential gel electrophoresis and mass spectrometry and found 48 altered proteins mainly related to cellular signaling, cytoskeletal organization, and carbohydrate/energy metabolism. Thus, our results indicate remarkable electrophysiological and molecular changes in the PFC related to acute systemic inflammation that may explain some of the concomitant behavioral and physiological symptoms.

1. Introduction

It has long been observed that acute systemic inflammation induces various neuropsychiatric symptoms both in humans and other mammals (Dantzer, 2004; Cunningham et al., 2009; Capuron and Castanon, 2016). One of the intensively studied behavioral effects of systemic infection is the manifestation of sickness behavior that resembles some features of human major depression (Dantzer et al., 2008). However, in addition to the well-described depression-like symptoms, there are other cognitive and behavioral effects of peripherally induced neuroinflammation that can be associated with functional disturbances in the central nervous system (CNS) (Cunningham and Sanderson, 2008; Mina et al., 2014;

* Corresponding author. ELTE NAP Neuroimmunology Research Group, Department of Biochemistry, Institute of Biology, ELTE Eötvös Loránd University, Budapest, Hungary.
E-mail address: kakekesi@ttk.elte.hu (K.A. Kékesi).
[1] These authors contributed equally to this work and share last authorship.

https://doi.org/10.1016/j.bbih.2023.100594
Received 3 October 2022; Received in revised form 12 December 2022; Accepted 16 January 2023
Available online 21 January 2023

Zhao et al., 2019). The majority of these neuropsychiatric changes are secondary to peripheral immune activation without direct CNS infection (Gofton and Young, 2012), highlighting the role of the underlying neuro-immune interactions that are only partially elucidated. The neurobiological alterations induced by systemic inflammation affect all aspects of brain function and are associated with many pathological conditions. The inflammatory response of the CNS is mediated by several resident and invading cell types; however, microglia play central role in the immune homeostasis of the brain (Skaper et al., 2018). These cells respond to immunological stimuli by the production of proinflammatory cytokines and chemokines and by increased migration and phagocytic activity (Woodburn et al., 2021). The inflammation-related changes of blood-brain barrier permeability also contribute to the elevated brain levels of proinflammatory mediators and to the infiltration of peripheral immune cells (Banks et al., 2015), further enhancing the inflammatory processes in the CNS parenchyma. Depending on the intensity and duration of the initial stimulus, this proinflammatory response results in widespread molecular and neurophysiological alterations (DiSabato et al., 2016). Increased inflammatory gene expression (Schwarz and Bilbo, 2011), cytokine-induced changes of neuronal excitability (Samios and Inoue, 2014), synapse loss (Xin et al., 2019), impaired synaptic plasticity (Rizzo et al., 2018), altered brain energy metabolism (Kealy et al., 2020), and increased neuronal death (Fan et al., 2015) have been observed under neuroinflammatory conditions. In addition, transcriptomic (Diaz-Castro et al., 2021), proteomic (Györffy et al., 2014), metabolomic, and lipidomic (Puris et al., 2022) changes have also been found in animal models of peripherally induced neuroinflammation. The complex interactions of these molecular and cellular effects may ultimately result in behavioral and cognitive changes, most of which are associated with the prefrontal cortex (PFC) (Miller, 2000; Kesner and Churchwell, 2011). Thus, it can be assumed that PFC dysfunctions also contribute to the CNS effects of peripheral immune activation. Indeed, microglial activation and upregulation of proinflammatory signaling (Ji et al., 2020; Jiang et al., 2022), alterations in excitatory and inhibitory neurotransmission (Feng et al., 2021; Jiang et al., 2022), and disturbances in oscillatory activity (Mamad et al., 2018; Ji et al., 2020) have been described in the PFC of rodents subjected to peripheral immune challenge. However, the physiological and molecular mechanisms underlying the neuroinflammation-related dysfunctions of the PFC are still unknown to a great extent. For this reason, we investigated the electrophysiological and proteomic alterations of the PFC using brain slices and the lipopolysaccharide (LPS) mouse model of acute peripheral infection.

It is well established that interleukin-1 beta (IL-1β), a key proinflammatory cytokine plays crucial role in neuroinflammatory processes (Basu et al., 2004; Pinteaux et al., 2009), e.g., in the CNS effects of peripheral LPS challenge (Sheppard et al., 2019; Zhao et al., 2020). IL-1β signal transduction requires the binding of IL-1β to its cell surface receptor (IL-1R1) and the subsequent recruitment of its coreceptor (IL-1RAcP) to form an activated IL-1R complex (Boraschi et al., 2018). This activated receptor complex initiates canonical IL-1 signaling, involving adaptor proteins (MyD88, Tollip), kinases (IRAKs, TAK1), and other enzymes (TRAF-6), which finally results in the activation of NFκB, p38 MAPK, and JNK pathways (Dinarello, 2009; Boraschi et al., 2018). As the components of the IL-1/IL-1R system are also expressed in neurons (Nguyen et al., 2011; Liu et al., 2019), IL-1 signaling can lead to changes in neuronal activity, which has already been described in some types of neurons (Ferri et al., 2005; Brambilla et al., 2010). Focusing on neuroinflammatory processes in the PFC, we examined the electrophysiological actions of IL-1β by patch clamp recordings of PFC pyramidal cells and interneurons. The bioinformatics analysis of our single-cell transcriptomic data (GEO accession number: GSE135060) revealed that the genes encoding IL-1R1 and IL-1RAcP show different degrees of coexpression in PFC pyramidal cells and interneurons. In turn, increased brain levels of IL-1β could change the excitatory and inhibitory balance in the PFC resulting in changes in oscillatory coupling between PFC and other cortical areas. To investigate the network-level consequences of acute systemic inflammation, frontal electroencephalographic (EEG) activity and fronto-occipital functional connectivity were analyzed in freely moving LPS-treated mice, as the alterations of fronto-occipital synchrony are associated with cognitive processes (Sauseng et al., 2005; Han et al., 2019) impaired by neuroinflammation. The LPS-induced increase of IL-1β and IL-1R1 levels in the PFC was measured by immunoassays, to integrate our *ex vivo* and *in vivo* data and to create a cellular and network-level model of IL-1β-related neurobiological alterations after peripheral inflammation.

Actual understanding of cognitive processes at synaptic level suggests complex molecular reorganization of the synaptic proteome under neuroinflammatory conditions. Plasticity of synaptic processes largely contribute to cognitive functions (Yan and Rein, 2021) and to neural oscillatory activity (Buzsáki et al., 2012), thus we assumed that peripherally induced neuroinflammation may cause complex changes in the synaptic proteome of the PFC. Therefore, we performed a proteomic analysis of synaptosome samples prepared from the PFC of control and LPS-treated animals and identified the altered proteins by mass spectrometry.

Taken together, the aim of the present study was to reveal neurobiological alterations in LPS-treated mice that may explain some of the behavioral and cognitive effects of acute systemic infection. Despite the clinical relevance of these neuropsychiatric symptoms of peripheral immune challenge, the underlying CNS mechanisms are not yet fully understood. In the present work we applied physiological and molecular approaches to reveal PFC mechanisms activated by peripheral inflammation, i.e., we revealed complex changes at molecular, cellular, and network-level that may contribute to the neuroinflammation-induced impairment of brain functions.

2. Materials and methods

2.1. Animals

Male C57BL/6N mice (Innovo Ltd., Isaszeg, Hungary) were housed under standard laboratory conditions (24 °C, 50–60% relative humidity, 12 h light/dark cycle) with *ad libitum* food and water access. All efforts were carried out to minimize the pain and suffering of animals and to reduce the number of animals used. All animal experiments were performed according to the regulations of the Animal Welfare Committee of Eötvös Loránd University, the EU Ethical Rules of Using Animals for Research Purposes (2010/63/EU revising Directive 86/609/EEC) and the Hungarian Act of Animal Care and Experimentation (1998, XXVIII). We performed our experiments with the permission of the Hungarian Scientific Ethics Council for Animal Experiments (license number: PE/EA/00513-6/2022). A total of 79 mice were used (n = 36 for *ex vivo* electrophysiology, n = 6 for *in vivo* electrophysiology, n = 25 for IL-1β and IL-1R1 immunoassays, and n = 12 for proteomic investigation) in the study. Animals were randomly assigned to experimental groups.

2.2. Peripheral induction of neuroinflammation

To model systemic bacterial infection, mice were injected intraperitoneally (i.p.) with a single dose of 2 mg/kg LPS (L2630, *Escherichia coli* (O111:B4), Sigma-Aldrich, St. Louis, MO, USA). We chose this relatively high dose based on previous publications (Batista et al., 2019; Zhao et al., 2020) to promote a rapid and intense systemic immune activation. The lyophilized LPS was dissolved in sterile saline (0.9% NaCl) at a concentration of 1.0 mg/ml and was stored in aliquots at −20 °C until use. Then it was diluted in 0.2 ml saline immediately before injection. As described for each experiment, mice were sacrificed 4, 6, 8, or 24 h after LPS administration. Control animals were injected i.p. with sterile saline (0.2 ml) and sacrificed 4 h after injection.

2.3. Electrophysiology

2.3.1. Ex vivo electrophysiology

Patch clamp experiments were performed in acute brain slices on a total of n = 63 cells prepared from n = 36 animals (4–5 weeks old). Mice were anesthetized with isoflurane, decapitated, and the brain was quickly removed and placed in ice-cold (0–4 °C) carbogenated (95% O_2, 5% CO_2), sucrose-based artificial cerebrospinal fluid (ACSF, composition in mM: 85 NaCl, 2.5 KCl, 2.0 $MgCl_2$, 1.125 NaH_2PO_4, 25 $NaHCO_3$, 25 glucose, 60 sucrose, 1.0 $CaCl_2$, pH 7.4) for 1–2 min. Then coronal slices (300 μm) containing the PFC were cut in the same ACSF using a vibratome (Leica VT1000 S, Leica Biosystems, Wetzlar, Germany). Slices were transferred to a recovery chamber submerged in carbogenated incubation ACSF (composition in mM: 125 NaCl, 2.5 KCl, 2.0 $MgCl_2$, 1.125 NaH_2PO_4, 25 $NaHCO_3$, 25 glucose, 1.0 $CaCl_2$, pH 7.4) and were incubated at room temperature (23–25 °C) for at least 1 h. After incubation, slices were transferred to a recording chamber and continuously superfused with heated (34 °C) and carbogenated experimental ACSF (composition in mM: 125 NaCl, 2.5 KCl, 1.0 $MgCl_2$, 1.125 NaH_2PO_4, 25 $NaHCO_3$, 25 glucose, 2.0 $CaCl_2$, pH 7.4) at a flow rate of 1.5–2.0 ml/min. The recording chamber was placed under an upright microscope (Leica DM6000 FS, Leica Mycrosystems) equipped with infrared/DIC optics. The whole apparatus was placed in a Faraday cage built on a vibration-free table. The patch clamp micropipettes (6.0–9.0 MΩ) were pulled from borosilicate glass capillaries (BF150-86-10, Sutter Instrument, Novato, CA, USA) and were filled with 8 μl of an internal solution (composition in mM: 130 potassium gluconate, 20 KCl, 10 HEPES, 0.16 EGTA, 4.0 ATP, 2.0 $MgCl_2$, 0.3 GTP, pH 7.4). Electrophysiological signals were amplified by a preamplifier (HS-2A Headstage, Axon Instruments, Union City, CA, USA) and by an AxoClamp-2B amplifier (Axon Instruments) connected to a signal conditioner (CyberAmp 320, Axon Instruments). Analog data were digitized at 10 kHz by a CED Micro1401 mk II data acquisition device (Cambridge Electronic Design, Cambridge, UK). For online data recording and offline analysis, we used CED Signal 4.11 software (Cambridge Electronic Design). The firing pattern of the recorded neurons was analyzed using a script of CED written for the evaluation of patch clamp data (Intracellular spike analysis, Cambridge Electronic Design, http://ced.co.uk/downloads/scriptsiganal). For somatic whole-cell patch clamp recordings pyramidal cells and interneurons were targeted in layer II/III and layer V of the medial PFC (mPFC, in the prelimbic, infralimbic, and medial orbital cortices according to Paxinos and Franklin, 2001). Neurons either having resting membrane potential more positive than −55 mV or showing resting membrane potential fluctuations higher than 15% were excluded from the experiments. To record neuronal firing, a current step protocol was applied by injecting 500 (pyramidal cells) or 300 (interneurons) ms long current pulses every 20 s in 50 pA increments starting at −100 pA. A medium current pulse was then selected for further stimulation (pyramidal cells: 168.52 ± 49.66 pA, interneurons: 603.33 ± 274.00 pA), at which cells fired stably at a medium frequency. This recording protocol was applied three times for each cell: for a baseline, a treatment, and a washout period. During the baseline period slices were superfused with experimental ACSF and neuronal firing was recorded for 5–6 min. This was followed by a 10 min treatment period while one of the following treatments was applied for pyramidal cells: ACSF alone as control (n = 7), 0.05 ng/ml recombinant IL-1β (10139-HNAE, Sino Biological, Beijing, China) (n = 7), 1 ng/ml IL-1β (n = 8), 20 ng/ml IL-1β (n = 9), 80 ng/ml recombinant interleukin-1 receptor antagonist (IL-1Ra, 200-01RA, Peprotech, Rocky Hill, NJ, USA) (n = 7), and 20 ng/ml IL-1β together with 80 ng/ml IL-1Ra (n = 7). Interneurons (fast-spiking and non-fast-spiking, altogether n = 9) were treated only with 20 ng/ml IL-1β. The applied concentrations of IL-1β and IL-1Ra were chosen based on previous publications (Viviani et al., 2003; Hoshino et al., 2017; Skelly et al., 2019) and the proteins were administered *via* the bath perfusion system. The treatment period was followed by a 10 min washout period while slices were superfused with ACSF alone again. ACSF contained 1 μg/ml BSA (A7030, Sigma-Aldrich) to reduce the nonspecific adsorption of IL-1β and IL-1Ra to surfaces. Considering the possible long-term effects of the administered proteins, only one neuron per slice was examined when IL-1β and/or IL-1Ra were applied. In another experiment, brain slices were obtained from mice injected with LPS 4 h before slice preparation. In the slices of LPS-treated animals we recorded only pyramidal cells (n = 9) without any additional treatment. After recordings, the threshold potential and latency of the first action potential, and the average firing frequency (Suppl. Fig. 1) were determined for each current step. Data from 5 to 10 steps were averaged for all three recording periods of each neuron.

2.3.2. In vivo electrophysiology

The surgical procedure and EEG recordings were carried out on n = 6 mice (3–6 months old). The anesthesia was induced by 4.0–5.0% Isoflurane and sustained by 2.0% (in air, 1.2 l/min). After the complete loss of consciousness, the fur of the scalp was shaved and mice were placed in a small animal stereotaxic instrument (Model 900, David Kopf Instruments, Tujunga, CA, USA) equipped with a mouse adaptor and a heating pad (adjusted to 37 °C). The skin was disinfected and cut in the midline to expose the skull. The skull was then cleaned with 3.0% H_2O_2 and four holes were drilled for the sterilized stainless steel screw electrodes (d = 1 mm), which were soldered pre-surgically to a piece of insulated wire. Two recording electrodes were implanted epidurally above the right frontal (2.6 mm anterior to bregma, 1.5 mm lateral to the midline) and occipital (2.7 mm posterior to bregma, 1.5 mm lateral to the midline) cortices, while the ground and reference electrodes were implanted above the right and left cerebellar hemispheres, respectively. All electrodes were then soldered to a 4-socket female connector that was fixed to the skull with dental cement. The skin was sutured and disinfected around the connector and lidocaine was administered locally to reduce post-surgical pain. The mice were rehydrated with sterile saline (0.2 ml, i.p.) and allowed a recovery period of 4–5 days before EEG recordings. The day before the experiments, freely moving mice were connected to the wire of a 4-channel differential preamplifier (Supertech, Pécs, Hungary) and placed individually in a Faraday cage for 1–2 h to habituate. Analog EEG signals were filtered (0.3 Hz–1.0 kHz) and amplified (gain: 5000) by a 4-channel biological amplifier (BioAmp, Supertech) and digitized (1.0 kHz, 16 bit) by a CED Micro1401-3 data acquisition unit (Cambridge Electronic Design). Online data recording and offline data preprocessing were performed using CED Spike2 8.04 software (Cambridge Electronic Design). EEG experiments were carried out on two consecutive days in a self-controlled manner. On the control day mice were injected i.p. with sterile saline at 10:00 a.m. and 20 min recordings were taken every hour until 06:00 p.m. The next day, mice were weighed and a 24 h post-injection control recording was performed at 10:00 a.m. Mice were then injected with LPS and recordings were taken with the same timing as control recordings (every hour from 10 a.m. to 6 p.m.). After the 24 h post-LPS recordings mice were sacrificed by an overdose of urethane. We analyzed and compared the data from recordings at 2, 4, 6, 8, and 24 h after saline and LPS injection. During the preprocessing of raw data, EEG signals were low-pass filtered at 200 Hz using a finite impulse response filter in CED Spike2 8.04. Filtered recordings were then thoroughly inspected visually and three artifact-free 30 s epochs were randomly excised from each recording file. Spectral analysis of the frontal EEG recordings was performed in the Signal Processing toolbox of OriginPro 8.5. (OriginLab Corporation, Northampton, MA, USA) by calculating power spectra (Hanning window, 1024 points). The following frequency bands were examined: delta (0.3–4 Hz), theta (4–12 Hz), low gamma (40–100 Hz), and high gamma (100–160 Hz). Fronto-occipital cross-correlation and coherence (Hanning window, 1024 points) were also calculated using OriginPro 8.5. Correlation and coherence are non-directed metrics of functional connectivity characterizing the similarity between two EEG signals in the time and frequency domains, respectively (Guevara and Corsi-Cabrera, 1996; Bastos and Schoffelen, 2016). Normalized cross-correlation can

be calculated as $y(m) = \sum_{i=0}^{M-1} f_{norm}(n) g_{norm}(n)$, where *y(m)* is the correlation coefficient, $f_{norm}(n)$ and $g_{norm}(n)$ are the normalized input signals of the same length (M). Correlation provides information about the time coupling and waveform similarity between two time series (Guevara and Corsi-Cabrera, 1996), in the present case, EEG signals. Its value can range from −1 to 1, where −1 means the perfect negative, while 1 means the perfect positive correlation of the two signals. The coherence of two waveforms (x and y) at frequency f can be defined as follows: $C_{xy}(f) = \frac{|P_{xy}(f)|^2}{P_{xx}(f)P_{yy}(f)}$, where P_{xy} is the cross-spectral density of the two signals, while P_{xx} and P_{yy} are the spectral densities of x and y, respectively. Coherence is the function of frequency and it quantifies the degree of variance in one of the signals that can be explained by the other signal (Bastos and Schoffelen, 2016). Its magnitude can range from 0 to 1. Zero indicates that the two signals are totally unrelated, while 1 indicates that the two signals are totally corresponding to each other at a given frequency. Before statistical analysis, Fisher z-transformation was performed to ensure the normal distribution of the coherence data. The EEG power and connectivity data from single epochs were averaged appropriately for every recording session.

2.4. IL-1β and IL-1R1 immunoassays

To investigate the neuroinflammation-induced changes of the prefrontal IL-1 system, PFC tissue homogenates were obtained from mice (3–6 months old) 4, 6, 8, and 24 h after the administration of LPS (n = 5 per group). Control samples were prepared 4 h after saline injection from n = 5 animals. Serum samples were also prepared to monitor changes in the peripheral levels of IL-1β. Mice were anesthetized with i.p. injected urethane (1.25 g/kg), the heart was exposed and blood was collected from the right ventricle. Mice were then transcardially perfused with normal saline (0.9% NaCl) until the liver lost its color. The brain was quickly removed, a coronal section was cut from the anterior part of the cerebral hemispheres, and PFC was dissected on ice using a fine curved forceps and a razor blade. PFC tissue samples were then halved, weighed, and immediately frozen on dry ice. One half of the PFC tissues was used for IL-1β and the other half for IL-1R1 immunoassays. To prepare serum samples, blood was allowed to clot for 30–40 min and centrifuged at 5000 rpm for 10 min at room temperature, and the serum fraction was collected and stored at −80 °C until use.

2.4.1. Magnetic bead-based immunoassay for serum and PFC IL-1β detection

PFC tissue homogenates were prepared according to the manufacturer's slightly modified protocol (MAN0017834, Thermo Fisher Scientific – Bender MedSystems GmbH, Vienna, Austria). One half of the PFC tissue samples was homogenized for 1 min in chilled cell lysis buffer (300 μl/100 mg of tissue, EPX-99999-000, Thermo Fisher Scientific) using a cordless motor (Z359971-1 EA, Sigma-Aldrich) with disposable pestles (BAF199230001-100 EA, Sigma-Aldrich) in 1.5 ml microcentrifuge tubes containing sample grinding resin (80-6483-37, GE Healthcare Bio-Sciences Corp., Piscataway, NJ, USA). Homogenized samples were then sonicated on ice three times for 10 s using an ultrasonic processor (CPX130PB, Cole-Parmer Instruments, Vernon Hills, IL, USA) at 20% of amplitude and 20 kHz frequency and centrifuged at 13,000 rpm for 15 min at 4 °C. The supernatant was collected and its total protein concentration was determined by the 2-D Quant Kit (80-6483-56, GE Healthcare), then samples were diluted to 10 mg protein/ml with 1X PBS. The concentration of IL-1β was measured in 25 μl of diluted PFC homogenates and serum samples using the ProcartaPlex Mouse Basic Kit (EPX010-20440-901, Thermo Fisher Scientific) and ProcartaPlex Mouse IL-1 beta Simplex Kit (EPX01A-26002-901, Thermo Fisher Scientific) according to the manufacturer's protocol. Samples were analyzed in a 96-well flat bottom plate by a Luminex MAGPIX instrument (Luminex Corporation, Austin, TX, USA) with xPONENT 4.2 software (Luminex Corporation). The MAGPIX platform operates on the principles of a sandwich ELISA; however, the capture antibody is bound to the surface of fluorescently dyed magnetic microspheres, enabling bead-based quantitative protein detection. The concentration of the analyzed protein was calculated by the software from standard curves using five-parameter logistic (5 PL) curve fitting.

2.4.2. Western blot analysis of PFC IL-1R1 expression

The other half of the PFC tissue samples were homogenized in 750 μl of chilled radioimmunoprecipitation assay (RIPA) buffer (150 mM NaCl, 1.0% Triton-X 100, 0.1% SDS, 50 mM Tris, pH 8.0) using a Dounce tissue grinder with B type (small clearance) pestle (Kontes Glass Co., Vineland, NJ, USA) for a total of 40 strokes. Seven and a half microliters of protease (P8340-5 ML, Sigma-Aldrich) and phosphatase (P5726-5 ML, Sigma-Aldrich) inhibitor cocktails were added to the RIPA buffer immediately before homogenization. Tissue homogenates were incubated in a Thermo-Shaker (TS-100, Biosan, Riga, Latvia) for 2 h at 4 °C and centrifuged at 13,000 rpm for 20 min at 4 °C. The supernatant was collected and its protein content was precipitated overnight by acetone at −20 °C. Next day, the samples were centrifuged at 13,000 rpm for 15 min and the protein precipitate was dissolved in lysis buffer (7.0 M urea, 2.0 M thiourea, 4.0% CHAPS, 20 mM Tris, 5.0 mM magnesium-acetate) by gentle sonication on ice. The total protein concentration of the samples was measured by the 2-D Quant Kit (GE Healthcare) and samples containing 70 μg protein were mixed with two-fold concentrated sample buffer (8.0% SDS, 3.0% DTT, 24% glycerol, 0.2% bromophenol blue, 100 mM Tris–HCl, pH 6.8) and incubated for 5 min at 96 °C. Proteins were separated on a discontinuous 10% polyacrylamide gel by Tricine-SDS electrophoresis (SE300 miniVE vertical electrophoresis system, Hoefer, Holliston, MA, USA) and transferred (MINIVE Blotter, Amersham Biosciences, Amersham, UK) onto a Hybond-LFP PVDF membrane (GE Healthcare). The blots were blocked with 5.0% BSA in Tris-buffered saline with 0.05% Tween-20 (TBS-T) for 1 h. The membranes were then incubated overnight at 4 °C in the blocking buffer with goat anti-IL-1R1 antibody (1:500 dilution, AF771-SP, R&D Systems, Minneapolis, MN, USA). Mouse anti-ATP1B1 antibody (1:1000 dilution, M17-P5-F11, Thermo Fisher Scientific) was used as loading control. Next day, the membranes were washed with TBS-T and incubated with anti-goat (705-545-147, Jackson ImmunoResearch, West Grove, PA, USA) and anti-mouse (715-585-151, Jackson ImmunoResearch) secondary antibodies diluted in TBS-T (1:800). After washing with TBS-T and then with TBS, the bands were visualized using a Typhoon TRIO + fluorescent laser scanner (GE Healthcare). Densitometry analysis of fluorescence signals was performed using the ImageJ software (https://imagej.nih.gov/ij/, National Institutes of Health, Bethesda, MD, USA). Densitometry data were normalized to the loading control.

2.5. Proteomic analysis of PFC synaptosomes

2.5.1. Synaptosome preparation

To investigate the synaptic proteome changes induced by peripherally evoked neuroinflammation, synaptosomes were prepared from the PFC of control (n = 6) and LPS-treated (n = 6) mice (3–6 months old) 4 h after saline or LPS injection, respectively. Mice were anesthetized with urethane, decapitated and the brain was quickly removed. PFC was then dissected on ice and the fraction of synaptosomes was prepared immediately following a routinely used protocol in our laboratory (Gulyássy et al., 2020; Tukacs et al., 2020), originally published by Phillips et al. (2001) and Hahn et al. (2009). Briefly, PFC tissue samples were homogenized with 40 strokes in a sucrose-based homogenization buffer (320 mM sucrose, 0.1 mM $CaCl_2$, 1.0 mM $MgCl_2$) using a Dounce tissue grinder with B type pestle (Kontes Glass Co.) at 4 °C. The chilled homogenization buffer was supplemented with protease and phosphatase inhibitor cocktails (Sigma-Aldrich). The homogenate was then adjusted to 1.25 M sucrose and 0.1 mM $CaCl_2$ in a final volume of 5 ml and was transferred to a centrifuge tube. Five milliliters of 1.0 M sucrose solution was layered on the samples and they were ultracentrifuged at 100,

000×*g* for 3 h at 4 °C. The fraction of synaptosomes was then collected as a band from the interface between the two sucrose layers, and its protein content was precipitated overnight by acetone at −20 °C. Next day, the protein precipitates were dissolved in lysis buffer by sonication on ice and samples were stored at −80 °C.

2.5.2. Two-dimensional differential gel electrophoresis (2-D DIGE)

The proteomic investigation of the synaptosome samples was performed by 2-D DIGE as described in our earlier publications (Szegő et al., 2010; Tukacs et al., 2020). Briefly, the pH of samples was adjusted to 8.0 and the total protein concentration was measured by the 2D-Quant Kit (GE Healthcare). The proteins were fluorescently labeled by a CyDye DIGE Fluor Labeling Kit for Scarce Samples (Cytiva, Marlborough, MA, USA). Samples containing 5 μg of proteins from LPS-injected and control mice were labeled with Cy3. The reference sample (pooled internal standard containing 2.5 μg of proteins from all samples) was labeled with Cy5. The differently labeled samples were then mixed and rehydrated passively onto 24 cm Immobiline DryStrip gels (pH 3–10 NL, GE Healthcare) overnight. Isoelectric focusing (IEF) was performed using an Ettan IPGphor 3 IEF unit (GE Healthcare) for 24 h to attain a total of 80-100 kVh. After IEF, the proteins were reduced with an equilibration buffer containing 0.1% mercaptoethanol. The separation of proteins by SDS-PAGE was performed on 24 × 20 cm, 10% polyacrylamide gels in an Ettan DALTsix Electrophoresis System (GE Healthcare). Following electrophoresis, gels were scanned in a Typhoon TRIO + scanner (GE Healthcare) using appropriate lasers and filters. We performed differential protein analysis with the DeCyder 2-D Differential Analysis Software package (GE Healthcare), using its Differential Analysis and Biological Variance Analysis modules. The fluorescence intensity of the Cy3 dye on a gel was normalized to the intensity of the Cy5 dye. The normalized fluorescence intensities of the protein spots were quantified and statistical analysis was performed using the DeCyder software. Protein spots, showing statistically significant alterations ($P < 0.05$ using independent, two-tailed Student's *t*-test) with more than ± 1.4 fold changes (FC), were selected for further protein identification by mass spectrometry. For the identification of proteins in these spots, preparative 2-D gel electrophoresis was performed separately with a total of 800 μg of proteins per gel. Resolved protein spots were stained with Colloidal Coomassie Brilliant blue G 250 (Merck Millipore, Billerica, MA, USA). The spots of interest were manually excised from the gels with pipette tips and placed in 1.0% acetic acid solution until protein identification.

2.5.3. Protein identification by mass spectrometry (MS)

Gel spots were destained using a 1:1 ratio of 25 mM ammonium bicarbonate pH 8.5 and 50% acetonitrile. The digestion was carried out overnight at 37 °C using 100 ng stabilized MS grade trypsin (Sciex, Framingham, MA, USA). The reaction was stopped by adding concentrated formic acid (Sigma-Aldrich) and peptides were extracted, dried in a speed-vac (Thermo Fisher Scientific), and kept at −20 °C until the analyses. Prior to mass spectrometry, peptides were separated on a 45-min water/acetonitrile gradient using an Easy nLC 1200 nano UPLC (Thermo Fisher Scientific). Buffer A was 0.1% formic acid in LC water (Sigma-Aldrich), solvent B was 95% acetonitrile (Sigma-Aldrich) with 0.1% formic acid. The flow rate was 300 nL/min. The desalting was done on an ACQUITY UPLC Symmetry C 18 trap column (20 mm × 180 μm, 5 μm particle size, 100 Å pore size, Waters, Milford, MA, USA) and the separation on an Acclaim PepMap RSLC C18 analytical column (150 mm × 50 μm, 2 μm particle size, 100 Å pore size, Thermo Fisher Scientific). Data-dependent analyses of the 14 most abundant positive ions were performed on an Orbitrap Fusion (Thermo Fisher Scientific) mass spectrometer (Orbitrap analyzer resolution: 60,000, AGC target: $4.0*10^5$, collision-induced dissociation in the ion trap with 35% normalized collision energy, AGC target: $2.0*10^3$, dynamic exclusion for 45 s). Protein identification was performed with MaxQuant 2.0.1.0 (Cox and Mann, 2008) and the UniProtKB *Mus musculus* database containing 17,119 mouse protein sequences (2021.09.29. release) was used. Oxidation of methionine, acetylation of the N-terminus, and carbamidomethylation of cysteine were set as variable modifications. Results were visualized in Scaffold 5.0.1 (Proteome Software Inc., Portland, OR, USA) and were manually curated. Those proteins were considered present for which a minimum of two peptides identified with at least 95% confidence were available.

2.5.4. Functional classification and bioinformatics analysis

Functional annotation and grouping of identified proteins were performed based on UniProtKB database (2022.02.01. release). Then, we applied ShinyGO 0.76 (Ge et al., 2020, http://bioinformatics.sdstate.edu/go/) to carry out enrichment analysis of the altered proteins with the mouse genome as background and with the FDR cutoff of 0.05. Top 30 enriched reactome terms were exported after removing redundant terms. Protein interactions between altered proteins were mapped using Metascape (Zhou et al., 2019, https://metascape.org) and visualized in Cytoscape 3.7.2 (Shannon et al., 2003). Edges with scores lower than 300 were excluded from the analysis. Nodes were colored based on FC values and their size represented eigenvector centrality (EC) calculated by CytoNCA app in Cytoscape. We carried out the clustering of the network with GLay clustering algorithm using the clusterMaker plugin. Enrichment analysis was then performed on each cluster using ShinyGO as described above. Top 20 enriched gene ontology (GO) biological process terms were exported after removing redundant terms. To find interactions between the altered proteins and IL-1 signaling, components of IL-1 signaling pathway were obtained from WikiPathways database (Martens et al., 2021, https://www.wikipathways.org) and STRING (Szklarczyk et al., 2021) was used to map their interactions with a combined score cutoff at 400. PathLinker Cytoscape app was used to find relations between the IL-1 pathway and altered proteins. Then, the obtained protein-protein interactions (PPIs) were merged with the signaling pathway and the PPIs of altered proteins. EC measures were calculated with the CytoNCA app and node degrees were plotted in relation to their eigenvectors in OriginPro 8.5.

2.6. Statistical analysis

The statistical analysis and the visualization of the results were carried out using OriginPro 8.5 and Origin 2018 software (OriginLab Corporation). The normal distribution of the data was confirmed by Shapiro-Wilk test before performing hypothesis testing. The statistical analysis of IL-1β patch clamp data was performed by one-way repeated measures ANOVA and by one-way ANOVA followed by Tukey *post hoc* test when a significant difference was found. The patch clamp data from the slices of control and LPS-treated mice were analyzed by two-sample *t*-test. The control and LPS treatment data from the EEG experiments were compared using the pair-sample *t*-test, while the results of IL-1β and IL-1R1 immunoassays were analyzed using two-sample *t*-test by comparing the control and 4 h LPS data. Statistical significance was accepted at the $P < 0.05$ level in each case. All data are expressed as mean ± standard deviation (SD) in both the text and the figures.

3. Results

As IL-1β plays key role in the regulation of neuroinflammation, we aimed to investigate its electrophysiological effects on pyramidal cells and interneurons in brain slices. First, we analyzed the single-cell sequencing data (GEO accession number: GSE135060) of our previous transcriptomic work (Ravasz et al., 2021) and found that the components of the IL-1β signaling system show different degrees of coexpression in pyramidal cells and interneurons of the murine PFC (Suppl. Fig. 2). The mRNA encoding IL-1R1 (*Il1r1*) was found in 16.95% of pyramidal cells and in 20.0% of interneurons, showing no significant differences in average copy numbers between the two cell types (pyramidal cells 0.70 ± 1.37; interneurons 1.49 ± 1.22; $t_{(13)} = 1.09$, $P = 0.29$,

two-sample *t*-test). However, the gene encoding IL-1RAcP (*Il1rap*), which is necessary for the CNS effects of IL-1β (Liège et al., 2000), was expressed by 27.12% of pyramidal cells and by only one (4.0%) interneuron, resulting in remarkably higher mRNA copy numbers in pyramidal cells (pyramidal cells: 27.92 ± 59.04, interneuron: 4.40). Thus, if this transcriptomic pattern correlates positively with the expression and distribution of the functional protein molecules, it can be assumed that pyramidal cells are more responsive to IL-1β.

3.1. *IL-1β enhances the intrinsic excitability of mPFC pyramidal cells under ex vivo conditions, whereas in vivo LPS treatment has no significant effects on pyramidal cell activity*

Examination of mPFC pyramidal cells by patch clamp recordings revealed that IL-1β enhances the intrinsic excitability of these cells in a concentration-dependent manner, which could be abolished by the co-application of IL-1Ra (Fig. 1). Control cells (superfused with ACSF) also showed some change in the threshold potential, firing frequency, and latency, which may be due to the recording procedure itself. However, these changes did not reach a significant level in either case (percentage changes are shown in Fig. 1B). Bath perfusion of 0.05 ng/ml IL-1β did not cause remarkable changes in threshold potential (baseline −38.67 ± 4.91 mV; treatment −37.72 ± 7.35 mV; washout −34.40 ± 11.90 mV; $F_{(2, 12)} = 1.31$, $P = 0.30$, one-way repeated measures ANOVA) and firing frequency (baseline 14.66 ± 5.21 Hz; treatment 17.05 ± 4.32 Hz; washout 14.75 ± 5.46 Hz; $F_{(2, 12)} = 1.41$, $P = 0.28$, one-way repeated measures ANOVA), but significantly reduced latency to 79.55 ± 6.20% of baseline, which persisted even during washout (baseline 44.60 ± 21.91 ms; treatment 35.79 ± 19.03 ms, $P = 0.032$; washout 36.08 ± 21.93 ms, $P = 0.038$; Tukey *post hoc* test after one-way repeated measures ANOVA, $F_{(2, 12)} = 5.49$, $P = 0.02$; Fig. 1B). Twenty-fold concentration (1 ng/ml) of IL-1β still did not cause a notable alteration in the threshold potential (baseline −43.21 ± 3.36 mV; treatment −44.95 ± 5.04 mV; washout −42.57 ± 7.20 mV; $F_{(2, 14)} = 1.00$, $P = 0.39$, one-way repeated measures ANOVA), but it significantly increased firing frequency to 138.09 ± 35.08% of baseline (baseline 11.86 ± 3.00 Hz; treatment 16.16 ± 4.74 Hz, $P = 0.0043$; washout 14.59 ± 4.97 Hz, $P = 0.064$; Tukey *post hoc* test after one-way repeated measures ANOVA, $F_{(2, 14)} = 7.79$, $P = 0.0053$) and decreased latency to 63.62 ± 20.32% of baseline, which could not be abolished by washout (baseline 39.03 ± 19.36 ms; treatment 25.32 ± 17.10 ms, $P = 0.0045$; washout 26.37 ± 15.50 ms, $P = 0.0075$; Tukey *post hoc* test after one-way repeated measures ANOVA, $F_{(2, 14)} = 11.07$, $P = 0.0029$; Fig. 1B). The highest applied concentration (20 ng/ml) of IL-1β irreversibly decreased the threshold potential to 89.48 ± 8.51% of baseline (baseline −40.42 ± 6.19 mV; treatment −44.43 ± 6.25 mV, $P = 0.0061$; washout −45.22 ± 5.94 mV, $P = 0.0014$; Tukey *post hoc* test after one-way repeated measures ANOVA, $F_{(2, 16)} = 10.83$, $P = 0.0011$), increased the firing frequency to 144.02 ± 36.73% of baseline (baseline 16.11 ± 7.62 Hz; treatment 21.51 ± 6.69 Hz, $P = 0.0016$; washout 20.82 ± 8.17 Hz, $P = 0.0049$; Tukey *post hoc* test after one-way repeated measures ANOVA, $F_{(2, 16)} = 10.82$, $P = 0.0011$), and decreased the latency to 57.06 ± 26.79% of baseline (baseline 31.12 ± 13.19 ms; treatment 18.36 ± 14.13 ms, $P = 0.00018$; washout 17.74 ± 13.36 ms, $P = 0.00011$; Tukey *post hoc* test after one-way repeated measures ANOVA, $F_{(2, 16)} = 20.16$, $P = 0.00004$; Fig. 1). The co-administration of IL-1Ra (80 ng/ml) with IL-1β (20 ng/ml) eliminated the excitatory effects of IL-1β on mPFC pyramidal cells (Fig. 1). Neither the threshold potential (baseline −37.02 ± 7.53 mV; treatment −38.79 ± 7.93 mV; washout −39.39 ± 8.82 mV; $F_{(2, 12)} = 3.16$, $P = 0.079$, one-way repeated measures ANOVA), nor the firing frequency (baseline 16.11 ± 8.00 Hz; treatment 18.50 ± 9.55 Hz; washout 17.22 ± 8.94 Hz; $F_{(2, 12)} = 3.66$, $P = 0.057$, one-way repeated measures ANOVA) showed significant alterations during the combined treatment. The analysis of latency data revealed a significant effect (baseline 41.54 ± 18.39 ms; treatment 36.56 ± 19.33 ms; washout 36.98 ± 21.38 ms; $F_{(2, 12)} = 4.08$, $P = 0.044$, one-way repeated measures ANOVA); however, the pairwise comparison did not confirm this result ($P = 0.059$, treatment compared to baseline; $P = 0.086$, washout compared to baseline, Tukey *post hoc* test). IL-1Ra alone, similarly to the control (ACSF) and combined (IL-1β + IL-1Ra) treatments, had no remarkable effects on pyramidal cell excitability (percentage data are shown in Fig. 1B). We compared the described effects of 20 ng/ml IL-1β and the effects of control and combined treatments and found that the percentage changes in threshold potential do not differ statistically between the treatments (ACSF 99.21 ± 6.60%; IL-1β 89.48 ± 8.51%; IL-1β + IL-1Ra 94.83 ± 7.69%; $F_{(2, 20)} = 3.17$, $P = 0.064$, one-way ANOVA). At the same time, changes in firing frequency (ACSF 119.51 ± 19.42%; IL-1β 144.02 ± 36.73%; IL-1β + IL-1Ra 106.66 ± 10.59%; $F_{(2, 20)} = 3.81$, $P = 0.041$, one-way ANOVA) and latency (ACSF 85.12 ± 21.13%; IL-1β 57.06 ± 26.79%; IL-1β + IL-1Ra 85.94 ± 14.28%; $F_{(2, 20)} = 4.61$, P

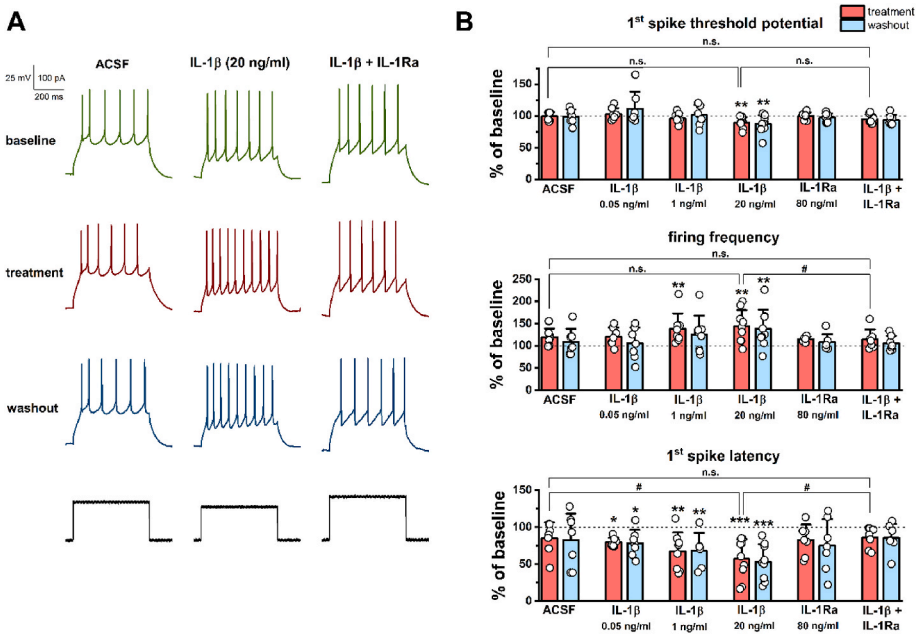

Fig. 1. IL-1β enhances the intrinsic excitability of mPFC pyramidal cells in brain slices. (A) Representative traces showing the baseline, treatment, and washout firing pattern of three mPFC pyramidal cells treated with ACSF, IL-1β (20 ng/ml), and IL-1β (20 ng/ml) together with IL-1Ra (80 ng/ml). (B) The percentage changes of the investigated parameters (n = 7–9 cells from 3 to 6 animals for each group). The threshold potential of the first spike showed a significant decrease during the treatment with 20 ng/ml IL-1β. However, this decrease was not significant compared to the slight changes induced by the control (ACSF) and combined (IL-1β + IL-1Ra) treatments (upper panel). Firing frequency showed a concentration-dependent increase induced by 1 ng/ml and 20 ng/ml IL-1β, which could be abolished by the co-application of IL-1Ra (middle panel). The latency of the first spike gradually decreased with the increasing concentrations of IL-1β, which was also prevented by IL-1Ra (lower panel). All observed changes were found to be irreversible during the 10 min washout period. One-way (#) and one-way repeated measures (*) ANOVA followed by Tukey *post hoc* test. Data are shown as mean ± SD. #, *$P < 0.05$; **$P < 0.01$; ***$P < 0.001$; n.s. not significant.

= 0.023, one-way ANOVA; Fig. 1B) show statistical differences between the treatments, i.e., these changes of pyramidal cell excitability may indeed have been caused by IL-1β acting *via* its receptor.

Next, we investigated whether an *in vivo* increase in the PFC levels of IL-1β (see section 3.5.) could cause similar changes in pyramidal cell excitability as the direct IL-1β treatment under *ex vivo* conditions. Therefore, brain slices were prepared from LPS-treated mice 4 h after injection and the activity of pyramidal cells was examined by patch clamp recordings (Suppl. Fig. 3). None of the excitability parameters showed a significant alteration; however, the tendency of changes was the same for all parameters as during *ex vivo* IL-1β treatment (Suppl. Fig. 3A). The threshold potential and the latency of the first spike decreased slightly, while the firing frequency increased compared to the control values. Furthermore, the rheobase also showed a moderate decrease after LPS treatment (for details see Suppl. Fig. 3B). Thus, LPS treatment 4 h before slice preparation does not appear to be sufficient to fully reproduce the *ex vivo* effects of IL-1β, but it slightly enhances pyramidal cell excitability.

3.2. IL-1β has no detectable effect on the intrinsic excitability of mPFC interneurons under ex vivo conditions

We next examined whether IL-1β applied *via* the bath perfusion system could have any effect on the intrinsic excitability of mPFC interneurons (fast-spiking and non-fast-spiking) in brain slices (Fig. 2). Because the highest dose of IL-1β (20 ng/ml) had the most significant effects on pyramidal cell activity, interneurons were treated only with this single dose (Fig. 2A). The results show that acute IL-1β treatment does not alter significantly either threshold potential (baseline −38.52 ± 7.65 mV; treatment −39.38 ± 8.41 mV; washout −38.03 ± 10.20 mV; $F_{(2,\ 16)} = 0.48$, $P = 0.63$, one-way repeated measures ANOVA), firing frequency (baseline 142.89 ± 89.58 Hz; treatment 144.48 ± 86.98 Hz; washout 142.71 ± 84.94 Hz; $F_{(2,\ 16)} = 0.078$, $P = 0.93$, one-way repeated measures ANOVA), or latency (baseline 8.69 ± 11.84 ms; treatment 7.61 ± 9.93 ms; washout 6.11 ± 7.87 ms; $F_{(2,\ 16)} = 2.37$, $P = 0.13$, one-way repeated measures ANOVA; percentage data are shown in Fig. 2B). Thus, the brain slice patch clamp recordings confirmed our previous single-cell mRNA sequencing data, i.e., the greater degree of coexpression of genes encoding the receptor (*Il1r1*) and coreceptor

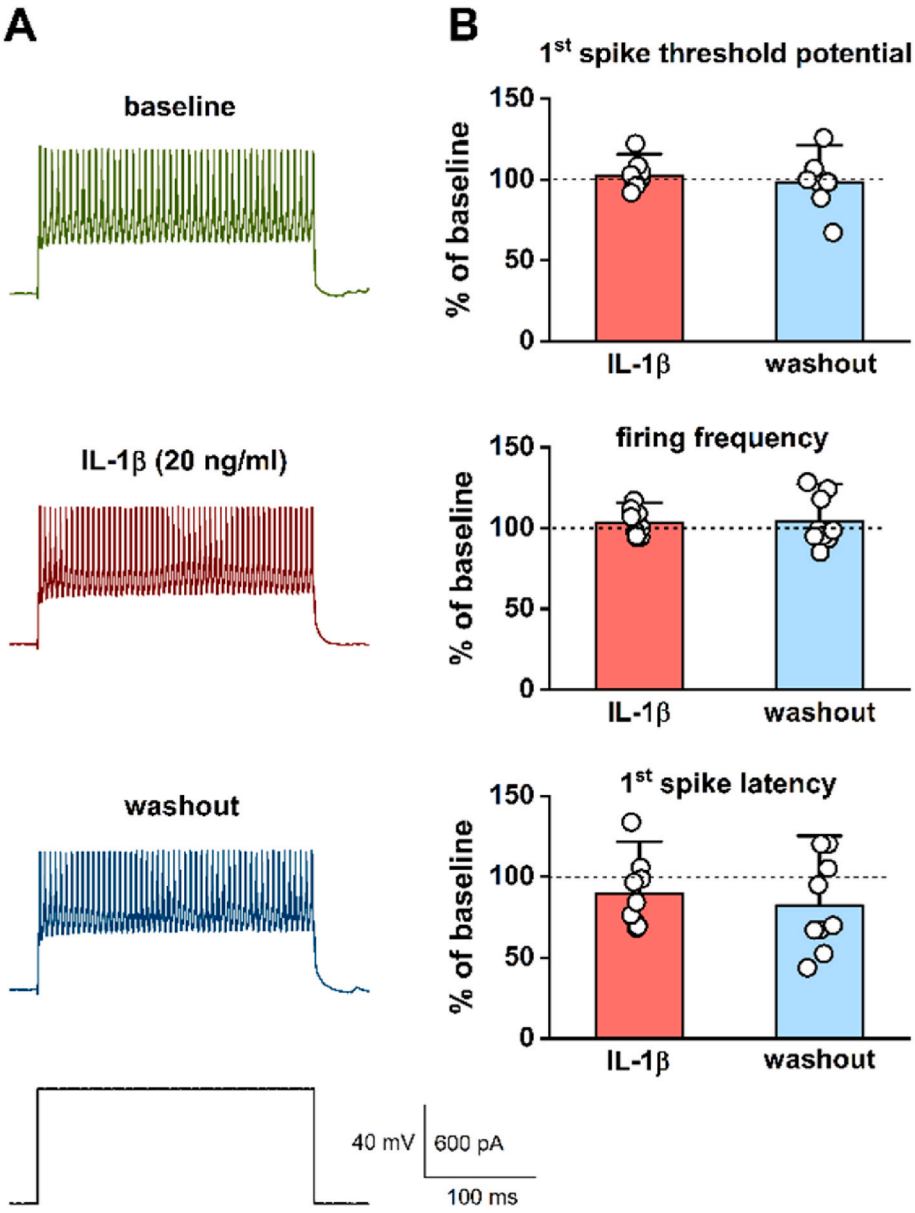

Fig. 2. IL-1β has no detectable effect on mPFC interneuron excitability under *ex vivo* conditions. (A) Representative traces showing the firing pattern of an mPFC fast-spiking interneuron during baseline (ACSF), treatment (20 ng/ml IL-1β), and washout (ACSF) recording periods. (B) Percentage changes of the investigated parameters show that IL-1β had no significant effect on the excitability of mPFC interneurons (n = 9 cells from 6 animals, one-way repeated measures ANOVA). Data are presented as mean ± SD.

(*Il1rap*) of IL-1β in mPFC pyramidal cells probably makes these cells more sensitive to the effects of IL-1β than interneurons.

3.3. Peripherally induced acute neuroinflammation causes altered neural oscillation in the frontal cortex

We investigated whether acute neuroinflammation altered neural oscillatory activity in the frontal cortex measured by epidural EEG recordings. As IL-1β, a major regulator of neuroinflammation seems to alter the electrical activity of cortical pyramidal cells and interneurons differently, LPS-induced neuroinflammation may cause detectable changes in EEG signals and functional connectivity metrics, since field potentials are spatio-temporal resultants of superimposed cellular electrical processes (Buzsáki et al., 2012). Representative EEG traces recorded after control and LPS treatment and average power spectra are shown in Suppl. Fig. 4. A general reduction could be observed in the power of the investigated EEG frequency bands at different time points after LPS treatment (Suppl. Fig. 5). Delta power showed a significant decrease 2, 4, 6, and 8 h after LPS injection, while theta and low gamma power decreased significantly 4, 6, and 8 h following the treatment. High gamma power was found to be significantly reduced only at 8 h after LPS treatment (for details see Suppl. Fig. 5). The peak frequency of the frontal EEG signals (full spectrum, 0.3–200 Hz) showed an increase at each time point after LPS injection (Suppl. Fig. 6); however, this increase was found to be significant only at 4 h after the induction of neuroinflammation (for details see Suppl. Fig. 6).

3.4. Neuroinflammation-induced changes in neural oscillation are associated with altered fronto-occipital functional connectivity

After analyzing the power and spectral changes of the frontal EEG signals, we investigated whether LPS-induced neuroinflammation could influence the fronto-occipital functional connectivity, since the alterations of fronto-occipital synchrony are associated with cognitive processes (Sauseng et al., 2005; Fingelkurts et al., 2007; Han et al., 2019) impaired by acute neuroinflammation. Thus, we calculated fronto-occipital cross-correlation (Fig. 3) and coherence (Fig. 4) based on control and post-LPS EEG data, which estimate the similarity of the two EEG signals in the time and frequency domains, respectively (for details see section 2.3.2.). As it can be seen in the fronto-occipital cross-correlograms (Fig. 3B), the degree of correlation at zero time lag increased at each time point after LPS treatment (major peak at 0 s time lag), reaching a significant level at 2 and 4 h (2 h: control 0.35 ± 0.14, LPS 0.47 ± 0.05, $t_{(5)} = -2.67$, $P = 0.044$; 4 h: control 0.36 ± 0.09, LPS 0.51 ± 0.05, $t_{(5)} = -3.40$, $P = 0.019$, pair-sample *t*-test; Fig. 3C). Moreover, in contrast to the asymmetric distribution of control correlation values, a more symmetric distribution and further minor correlation peaks with different time lags were detected at 2, 4, and 6 h after LPS treatment (Fig. 3B). These neuroinflammation-related changes were no longer clearly detectable at 24 h after the LPS treatment.

Based on the fronto-occipital coherence spectra (Fig. 4A), it can be seen that the degree of coherence increased mainly in the delta and high gamma frequency bands after LPS treatment. The increase in delta coherence was significant at 2 and 4 h (2 h: control 0.23 ± 0.11, LPS 0.31 ± 0.06, $t_{(5)} = -2.60$, $P = 0.048$; 4 h: control 0.20 ± 0.09, LPS 0.36 ± 0.05, $t_{(5)} = -3.70$, $P = 0.014$, pair-sample *t*-test), while the increase in

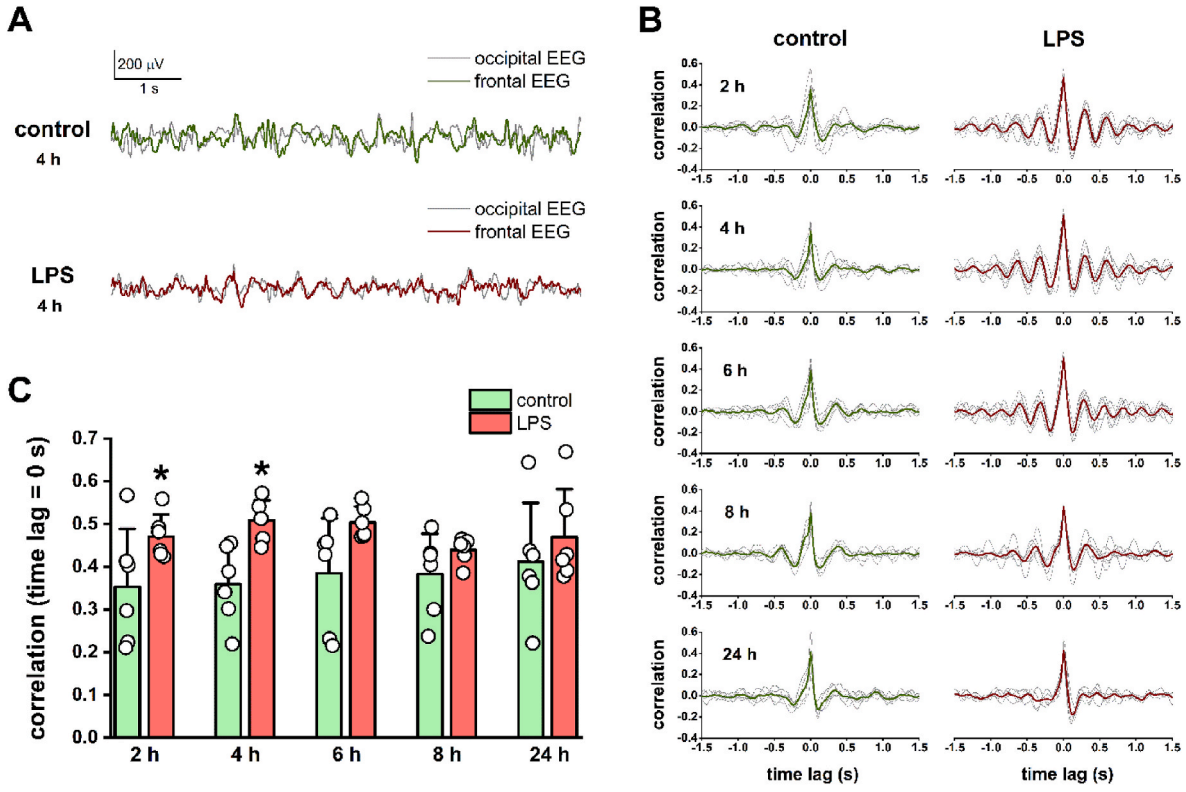

Fig. 3. LPS treatment induces alterations in the fronto-occipital EEG correlation. (A) Superimposed frontal and occipital EEG traces are shown at 4 h after saline and LPS injection. A decrease in signal amplitude and an increasing similarity of frontal and occipital waveforms can be seen under neuroinflammatory conditions. (B) Fronto-occipital cross-correlograms calculated from EEG data at different time points after saline and LPS injection. Data for each animal are shown in the background as thin gray lines, while the means of 6 animals are indicated by thick colored lines. Note the increasing symmetry of the correlograms and the appearance of additional correlation peaks beyond the major peak at 0 s time lag after LPS treatment. The observed changes are no longer detectable 24 h after the treatment. (C) The fronto-occipital cross-correlation calculated at 0 s time lag showed a significant increase 2 and 4 h after LPS injection (pair-sample *t*-test, n = 6). Data are presented as mean ± SD. *$P < 0.05$.

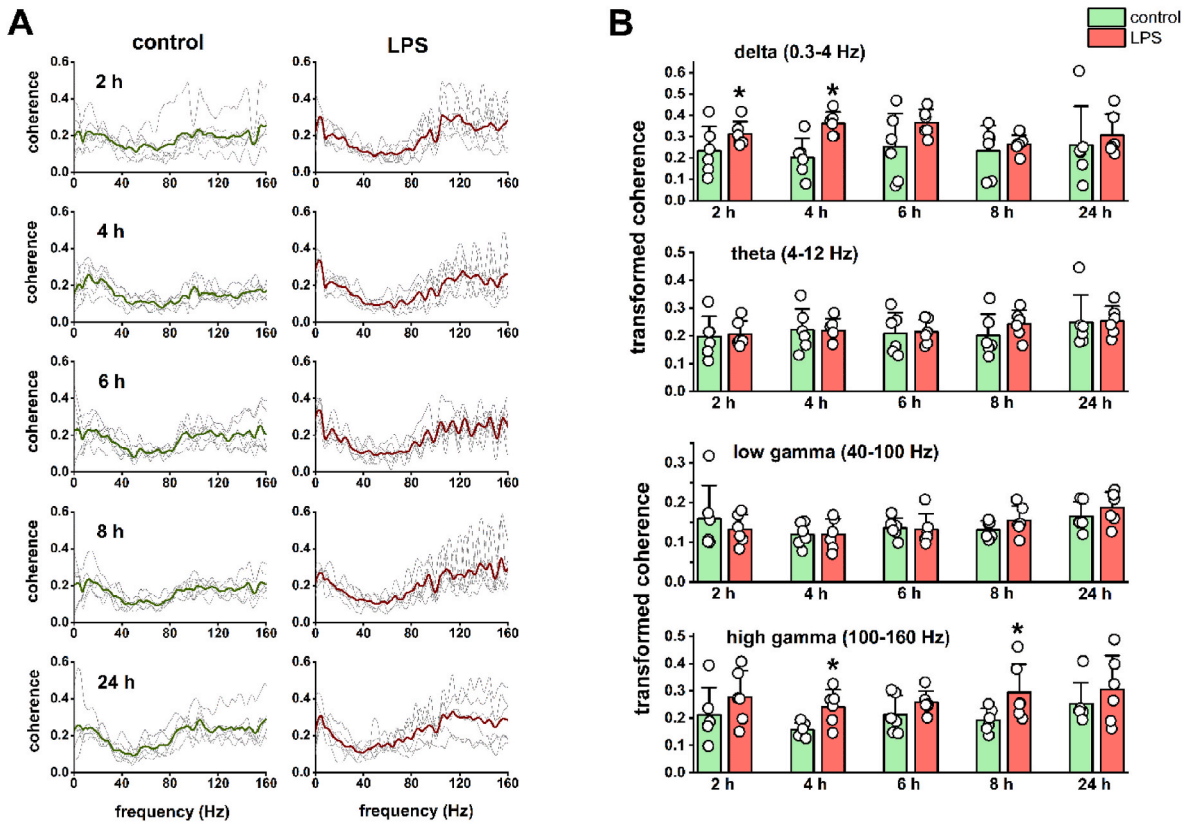

Fig. 4. LPS treatment results in increased fronto-occipital EEG coherence in the delta and high gamma frequency bands. (A) Fronto-occipital coherence spectra calculated from EEG recordings at different time points after saline and LPS injection. Coherence data for each animal are shown in the background as thin gray lines, while the means of 6 animals are indicated by thick colored lines. An increase in delta and high gamma EEG coherence can be observed 2–8 h after the LPS treatment. (B) Average z-transformed fronto-occipital coherence values for the investigated EEG frequency bands. Delta coherence (upper panel) increased significantly 2 and 4 h after LPS treatment, while high gamma coherence (lower panel) showed a significant increase 4 and 8 h after the treatment (pair-sample *t*-test, n = 6). Theta and low gamma coherence (middle panels) did not show remarkable changes related to neuroinflammation. Data are shown as mean ± SD. $^*P < 0.05$.

high gamma coherence was significant at 4 and 8 h (4 h: control 0.16 ± 0.03, LPS 0.24 ± 0.06, $t_{(5)} = -3.91$, $P = 0.011$; 8 h: control 0.19 ± 0.04, LPS 0.29 ± 0.10, $t_{(5)} = -3.38$, $P = 0.020$, pair-sample *t*-test; Fig. 4B) after the induction of inflammation. Theta and low gamma coherence did not show remarkable changes associated with LPS treatment (Fig. 4B). Similar to the correlation, differences in coherence between

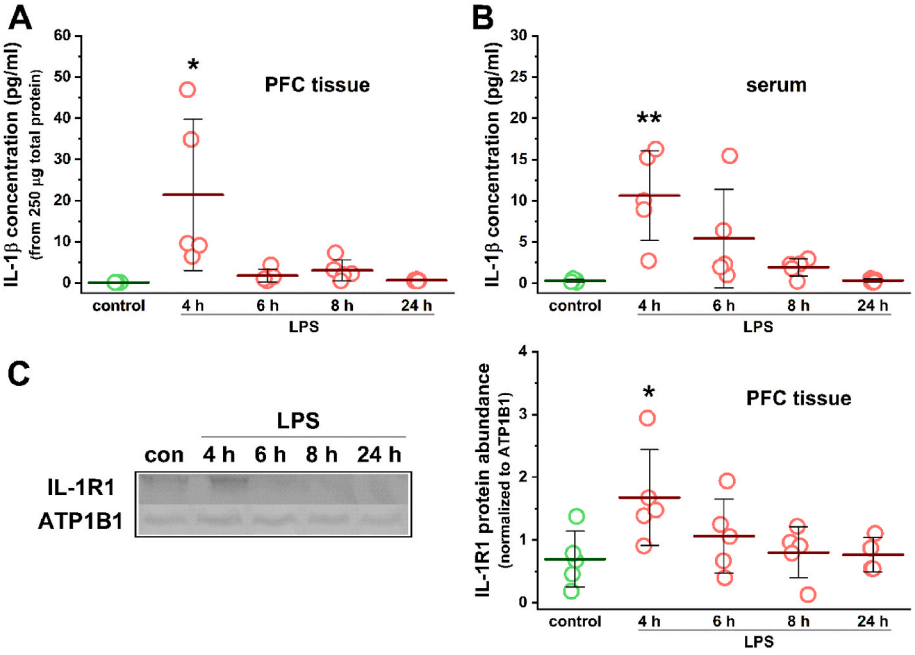

Fig. 5. The upregulation of IL-1β and IL-1R1 after LPS treatment shows a similar time course as the neuroinflammation-related EEG changes. (A) The concentration of IL-1β measured in PFC tissue homogenates at different time points after LPS injection. The data show a significant increase 4 h after the treatment and then a rapid decrease. (B) Serum levels of IL-1β also showed a significant increase 4 h after LPS injection; however, the following decrease was more gradual over time. The concentration of IL-1β was measured by a magnetic bead-based immunoassay. (C) Western blot analysis of PFC IL-1R1 expression after LPS treatment. Densitometry analysis of immunoblots from PFC tissue homogenates (left panel) revealed a significant increase in IL-1R1 levels at 4 h after LPS treatment and then a gradual decrease over time (right panel). Control and 4 h LPS data were statistically compared using two-sample *t*-test (n = 5 mice for each group). Data are presented as mean ± SD. $^*P < 0.05$, $^{**}P < 0.01$.

control and post-LPS recordings were largely reduced 24 h after the treatment. Thus, most of the neuroinflammation-induced changes in the power and spectral properties of frontal EEG, and in the fronto-occipital functional connectivity could be detected at early time points after LPS treatment (mostly around 2–4 h, but within the first 8 h), which is comparable to the time course of sickness behavior in rodents induced by systemic inflammation (Albrecht et al., 2018; Feng et al., 2021).

3.5. *The LPS-induced upregulation of the prefrontal IL-1 system follows a similar time course as most of the observed EEG changes*

To confirm the increase of prefrontal IL-1β levels in the murine neuroinflammation model we used and to investigate its time course, the concentration of IL-1β was measured in PFC tissue homogenates prepared from control and LPS-treated animals using a magnetic bead-based immunoassay (Fig. 5A). In the control samples the concentration of IL-1β was below the lower limit of quantitation of the assay (0.98 pg/ml); however, the software performed an automatic extrapolation

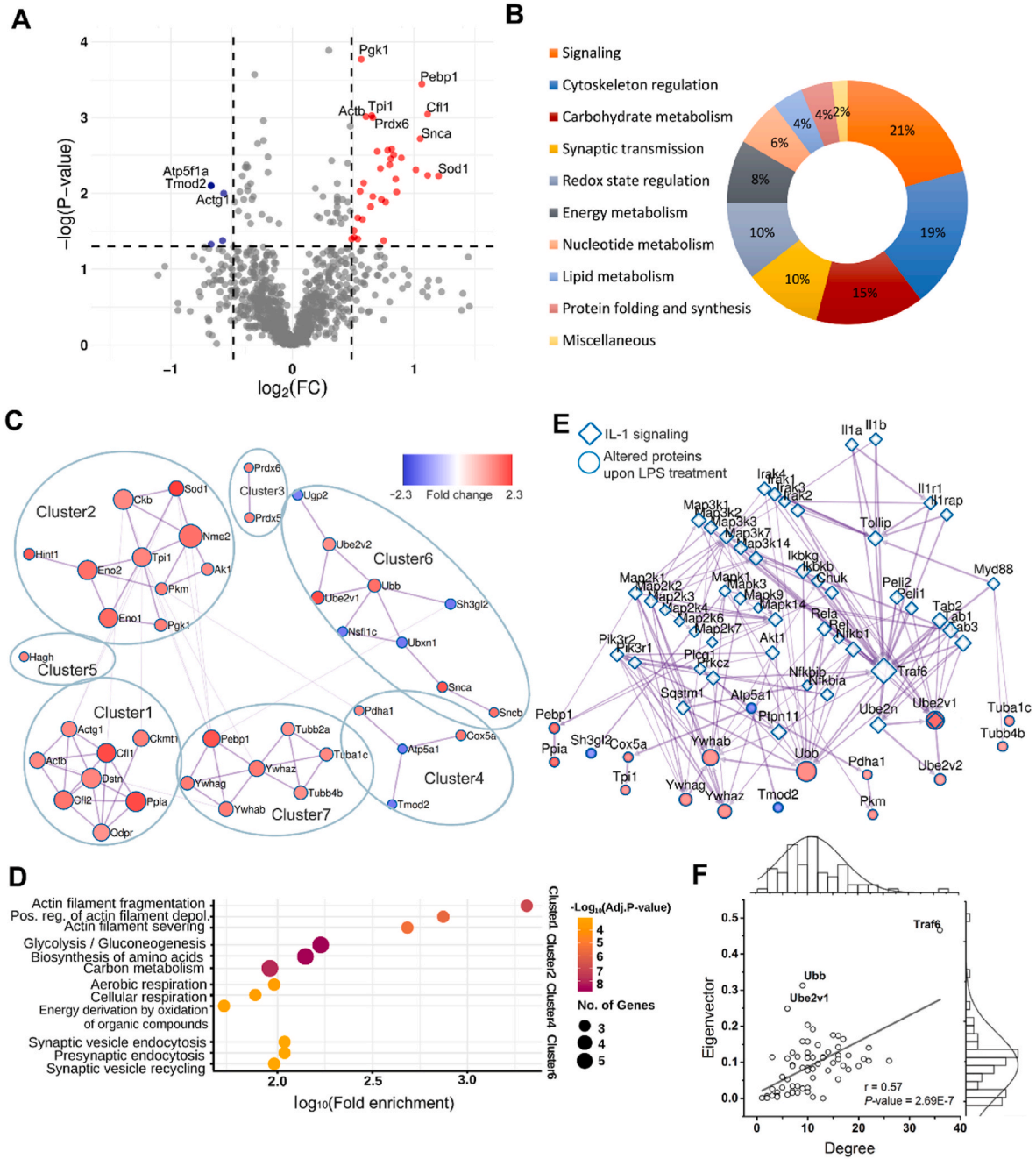

Fig. 6. LPS-induced proteomic alterations of PFC synapses reflect signaling, cytoskeletal, and metabolic changes. (A) Volcano plot shows significantly altered protein spots from PFC synaptosome samples (red – increased, blue – decreased) with labels of identified proteins (FC: fold change). (B) Pie chart shows the functional groups of identified proteins. (C) Clustered PPI network of altered proteins in response to LPS treatment. Nodes are colored based on FC, and their size represent eigenvector centrality (EC). (D) Top 3 enriched GO biological process terms for Cluster1, 2, 4, and 6. The number of related genes correlates with circle sizes, adjusted *P*-value is represented by color scales. (E) The PPI network of altered proteins linked to IL-1 signaling pathway. Nodes are colored based on FC, and their size represent EC. (F) Scatter plot of node degree and eigenvector of the linked PPI network. Pearson's correlation analysis and ANOVA test were performed, proteins with outstanding centrality index are labeled. (For interpretation of the references to color in this figure legend, the reader is referred to the Web version of this article.)

based on the detected fluorescence intensity values and took the concentration of IL-1β to 0.12 pg/ml in each sample. Compared to this, the IL-1β concentration showed a significant increase in the samples prepared 4 h after LPS treatment (21.37 ± 18.34 pg/ml, $t_{(8)} = -2.59$, $P = 0.032$, two-sample *t*-test). IL-1β levels in the PFC then decreased rapidly, as the values measured in the LPS 6, 8, and 24 h samples did not show remarkable differences from the control data (6 h: 1.78 ± 1.50 pg/ml; 8 h: 3.05 ± 2.56 pg/ml; 24 h: 0.64 ± 0.17 pg/ml, extrapolated; Fig. 5A). Serum IL-1β concentrations showed a similar pattern, as a significant elevation was found 4 h after LPS injection (control: 0.31 ± 0.16 pg/ml, extrapolated; 4 h: 10.64 ± 5.45 pg/ml, $t_{(8)} = -4.24$, $P = 0.0029$, two-sample *t*-test; Fig. 5B). However, serum levels of IL-1β decreased much slower over time compared to PFC levels, as slightly elevated concentrations were measured in the LPS 6 and 8 h samples (6 h: 5.43 ± 5.97 pg/ml; 8 h: 1.93 ± 1.04 pg/ml), which returned to the control levels only 24 h after LPS treatment (24 h: 0.36 ± 0.18 pg/ml, extrapolated; Fig. 5B). The Western blot analysis of PFC IL-1R1 expression also revealed a similar time course (Fig. 5C). A significant elevation was found 4 h after LPS injection (control: 0.69 ± 0.45, normalized protein abundance; 4 h: 1.68 ± 0.70, $t_{(8)} = -2.49$, $P = 0.038$, two-sample *t*-test), which gradually decreased over time toward control levels (6 h: 1.06 ± 0.59; 8 h: 0.80 ± 0.41; 24 h: 0.77 ± 0.27; Fig. 5C). Thus, the upregulation of the prefrontal IL-1 system appears to take place rapidly after the induction of neuroinflammation, which roughly overlaps in time with the *in vivo* electrophysiological changes described in the previous section.

3.6. The LPS-induced protein changes of PFC synapses are mainly related to cellular signaling, cytoskeletal organization, and carbohydrate metabolism

We detected 1330 protein spots in the 2-D gels of synaptosome fraction of the murine PFC (Suppl. Fig. 7). We could identify 48 proteins from 38 significantly altered spots with absolute fold changes (FC) above 1.4 ($P < 0.05$; independent, two-tailed Student's *t*-test) (Suppl. Table 1). The vast majority (42) of the identified proteins can be found in the SynProt database (https://synprot.de), which contains manually added proteomic data of mouse, rat, and human synaptic samples. Fluorescence intensity changes of protein spots varied between −1.59 and 2.3. Most of the spots (33) showed an intensity increase and only 5 showed a decrease in response to LPS-induced neuroinflammation (Fig. 6A). The spot with the highest alteration contained superoxide dismutase [Cu–Zn] (Sod1) (FC = 2.3; $P = 0.0059$). We found 2 spots with the FC of 2.16; they contained ubiquitin-conjugating enzyme E2 variant 1 (Ube2v1), cofilin-1 (Cfl1), CB1 cannabinoid receptor-interacting protein 1 (Cnrp1), and Sod1. In addition, we found 3 spots with FC of −1.59; they contained ATP synthase subunit alpha (Atp5f1a), tropomodulin-2 (Tmod2), actin 1 (Actb), NSFL1 cofactor p47 (Nsfl1c), UBX domain-containing protein 1 (Ubxn1), prostaglandin reductase 2 (Ptgr2), and endophilin-A1 (Sh3gl2). Functional annotation revealed a high ratio of signaling proteins (n = 10, 21%) and cytoskeleton regulators (n = 9, 19%) among the significantly altered proteins (Fig. 6B). We found 7 altered proteins associated with carbohydrate metabolism (15%), and most of them increased compared to control samples, such as gamma-enolase (Eno2), phosphoglycerate kinase 1 (Pgk1), pyruvate dehydrogenase E1 component subunit alpha (Pdha1), pyruvate kinase (Pkm), and triosephosphate isomerase (Tpi). We identified 5-5 (10-10%) proteins that regulate redox state and synaptic transmission. All the redox state regulators increased, such as Sod1, peroxiredoxin-5, and -6 (Prdx5, Prdx6). In addition, most of the proteins of synaptic transmission increased as well, such as Cnrp1, alpha-, and beta-synuclein (Snca, Sncb); only Sh3gl2 level decreased in this functional group. Four, 3, and 2 proteins were related to energy metabolism (8%), nucleotide metabolism (6%), and lipid metabolism (4%), respectively. Protein folding and synthesis had 2 related proteins (4%), and we found 1 miscellaneous protein (2%). Overrepresented reactome terms were identified by enrichment analysis of the altered proteins (Suppl. Table 2). The top five enriched reactome terms comprised FOXO transcription factor-, and apoptosis-related pathways; the related signaling proteins of these terms were 14-3-3 protein beta/alpha, zeta/delta, and gamma. Metascape mapped 71 interactions between 41 altered proteins with scores above 300. GLay clustering algorithm identified 7 clusters in this PPI network (Fig. 6C). We carried out GO enrichment analysis on each cluster (Fig. 6D, Suppl. Table 3). Cluster1 was enriched in actin filament organization-related terms; in Cluster2, proteins related to glycolysis/gluconeogenesis and biosynthesis of amino acids were overrepresented. Cluster4 and Cluster6 were enriched in terms associated with cellular respiration and synaptic transmission, respectively. Finally, we did not find significant or biologically relevant enriched terms in Cluster3, 5, and 7. We attempted to link the PPI network of the altered proteins to the PPI network of the canonical IL-1 signaling pathway, and we found one shared protein, namely Ube2v1, and several interactions between the two PPI networks (Fig. 6E). Average EC and degree of the merged PPI network were 0.091 and 10.7, respectively. Plotting the EC value and the degree of all nodes, 3 nodes had at least one outstanding centrality index (Fig. 6F); these were Ube2v1 (EC = 0.25, degree = 6), Ubb (EC = 0.31, degree = 9), and Traf6 (EC = 0.47, degree = 36). In conclusion, these results suggest that peripheral LPS treatment induced a widespread proteomic response in PFC synapses, which can be related to cellular/synaptic signaling, cytoskeletal organization, and metabolic processes. Moreover, the observed proteomic changes may also be associated with the proinflammatory signaling induced by IL-1β.

4. Discussion

4.1. IL-1β-induced changes of neuronal excitability and their possible effects on cortical excitatory/inhibitory balance

Several effects of IL-1β on neuronal electrophysiology have been revealed by *ex vivo* and *in vitro* studies focusing on different types of CNS neurons. It was shown in brain slices that IL-1β reduces the firing rate of cholinergic brainstem neurons (Brambilla et al., 2010), depolarizes and enhances the firing rate of hypothalamic neurons (Ferri et al., 2005), and hyperpolarizes and decreases the input resistance and spike threshold of thalamic relay cells (Samios and Inoue, 2014). In neuronal cultures from the hypothalamus IL-1β was found to hyperpolarize a subset of neurons and to decrease their input resistance and firing rate (Tabarean et al., 2006). A similar hyperpolarizing effect was described in cultured neurons from the subfornical organ, when IL-1β was applied in septic concentrations; contrarily, subseptic concentrations induced transient depolarization and increased firing frequencies (Desson and Ferguson, 2003). Thus, it can be seen that the excitatory or inhibitory nature of IL-1β-induced effects is largely neuron type-specific and may be concentration-dependent. Similarly, our results show that IL-1β acts in a cell-type specific manner on mPFC neurons, which may be due to the differential expression of the coreceptor of IL-1β in pyramidal cells and interneurons. Namely, the gene of IL-1RAcP was expressed almost exclusively by pyramidal cells and IL-1β-induced electrophysiological effects were also detected in these cells. The exact molecular mechanisms underlying these effects are not yet fully understood; however, the modifications of voltage- and ligand-gated ion channels and ion pumps by the PI3–K/Akt pathway (Diem et al., 2003), PKC and p38 MAPK (Zhou et al., 2011), and Src family kinases (Ghosh et al., 2016; Viviani et al., 2003) can be strongly assumed. These molecular processes are probably activated through IL-1R1 signaling, since the majority of IL-1β-induced electrophysiological effects depend on IL-1R1 activation and/or can be abolished by IL-1Ra (Desson and Ferguson, 2003; Diem et al., 2003; Tabarean et al., 2006; Zhou et al., 2011). Our present data show a slight enhancement of pyramidal cell excitability in brain slices of LPS-treated animals; however, these changes did not reach a significant level. Feng et al. (2021) reported similar results, as it was found that the excitability of pyramidal cells was not affected by a single dose of

LPS injected before slice preparation. Our observations may be explained by the fact that PFC IL-1β levels induced by *in vivo* LPS treatment (<50 pg/ml, Fig. 5A) are lower than the concentrations used in our patch clamp experiments (0.05–20 ng/ml). However, it should be mentioned that brain tissue levels of cytokines can also be altered by the mechanical and physiological effects of brain slice preparation and incubation (Jankowsky et al., 2000).

Thus, the question arises whether peripherally induced neuroinflammation can cause excitatory/inhibitory imbalance in cortical networks through its different effects on glutamatergic and GABAergic processes. Our patch clamp results suggest that neuroinflammation may induce excitatory/inhibitory imbalance *via* the different actions of IL-1β on the intrinsic excitability of pyramidal cells and interneurons, while Jiang et al. (2022) have reported alterations in synaptic electrical activity. The authors found that in the PFC slices of LPS-treated mice glutamatergic (but not GABAergic) neurons show increased inhibitory postsynaptic currents, resulting in an enhanced GABAergic tone on these cells. In addition, it was also reported that LPS treatment reduces the peak frequency of delta waves in the mPFC (Jiang et al., 2022). Contrarily, we found an increased peak frequency in the delta range after LPS injection; however, in the cited study recordings were performed under urethane anesthesia and a lower dose of LPS was administered. The results of Feng et al. (2021) also suggest the neuroinflammation-induced enhancement of inhibitory processes, as it was reported that LPS treatment before slice preparation increases the intrinsic excitability of fast-spiking interneurons in the prelimbic area of the mPFC. On the other hand, LPS treatment on three consecutive days reduced the expression of parvalbumin and decreased the intensities of vesicular GABA transporter and parvalbumin buttons in the mPFC, which proposes the weakening of cortical inhibition (Ji et al., 2020). Similar to our results, the latter work also revealed a general decrease in field potential power; however, these changes were not significant. Taken together, it can be seen that peripherally induced neuroinflammation can alter the intrinsic and/or synaptic excitability of PFC pyramidal cells and interneurons differently, depending on the dose of LPS, the duration of treatment, and the time after administration, ultimately resulting in excitatory/inhibitory imbalance and thus network-level disturbances. The excitatory/inhibitory imbalance in stress-sensitive brain regions (e.g., mPFC) has been associated with depression-like behavior (Ghosal et al., 2017; Wang et al., 2019), which shares many similarities with inflammation-related sickness behavior.

4.2. Neuroinflammation-related alterations of fronto-occipital functional connectivity

Fronto-occipital connectivity has been shown to play role in working memory (Sauseng et al., 2005), sleep-wake regulation (Gennaro et al., 2004), sustained attention (Han et al., 2019), and sensory information processing (Kunicki et al., 2019). As peripherally induced neuroinflammation is associated with the impairment of these neurophysiological and cognitive functions, it can be assumed that fronto-occipital coupling is also affected by acute systemic inflammation. To examine this issue, fronto-occipital EEG correlation and coherence were calculated from control and post-LPS recordings. Both metrics suggest a significant increase in fronto-occipital functional connectivity within the first 8 h after LPS treatment. Contrarily, it was found in LPS-treated rats that neuroinflammation reduces intra-hemispheric connectivity in the alpha, beta-gamma and high frequency oscillations bands (Albrecht et al., 2018). However, in this study connectivity was analyzed using the debiased weighted phase lag index, which is based on phase synchronization methods and is less sensitive to the effects of volume conduction and to the use of a common reference electrode. On the other hand, EEG correlation and coherence may indeed introduce spurious connectivity values (Bastos and Schoffelen, 2016), but it is also known that these metrics are nevertheless suitable for detecting direct causal interactions (Silfverhuth et al., 2012). Furthermore, as we focused on connectivity differences between control and post-LPS recordings, it can be strongly assumed that the described changes of fronto-occipital connectivity reflect real biological processes related to neuroinflammation. E.g., the increasing symmetry of fronto-occipital cross--correlograms after LPS treatment (Fig. 3B) may indicate that the normal flow of sensory information from visual to prefrontal cortex (Siegel et al., 2015) is impaired and the temporal functioning of the two cortical areas becomes much more similar; at the same time, the increased coherence in the high gamma range may be related to the imbalanced interplay of interneurons and pyramidal cells induced by proinflammatory signaling. Increased cortical functional connectivity has been reported in major depression (Fingelkurts et al., 2007; Olbrich et al., 2014), while the synaptic-level impairment of oscillatory synchronization between the hippocampus and mPFC has been observed in a rat model of depression (Zheng and Zhang, 2015). Thus, our results regarding changes in fronto-occipital connectivity can be probably also associated with the behavioral and cognitive disturbances related to neuroinflammatory conditions. No direct causal relationship was shown between IL-1β signaling and LPS-induced EEG and connectivity alterations; however, based on the *ex vivo* effects of IL-1β (Figs. 1 and 2) and the upregulation of the IL-1 system at nearly the same time as EEG changes (Fig. 5), it cannot be ruled out that the activation of IL-1β signaling is related to the observed *in vivo* electrophysiological changes. As in many other studies, we measured quantitative changes of IL-1β and IL-1R1 in tissue homogenates, which, however, reveals nothing about the exact distribution and cellular sources of these proteins within the PFC (i.e., these data represent the average tissue levels of the proteins). Furthermore, the age difference between the animals in each experimental group may also have biological effects, which can be manifested, e.g., in the relatively high SD values observed in some cases. Thus, the mechanistic interpretation of such results should be performed critically.

4.3. LPS-induced proteomic changes of PFC synapses

Our proteomic results indicate elevation of several functional protein groups in response to LPS treatment (Fig. 6), such as proteins related to glycolysis, redox state regulation, actin filament fragmentation, and several signaling proteins. In the whole PFC tissue of LPS-treated mice mainly proteins associated with energy and nucleic acid metabolism showed an increase (Wang et al., 2016), suggesting that neuroinflammation-related alterations of cellular signaling and cytoskeletal organization are more related to the synaptic compartment. In accordance with our results, increased levels of ROS and redox signaling in LPS-treated mice (Li et al., 2021) and a metabolic switch to glycolysis were shown in murine macrophages upon LPS treatment (Vijayan et al., 2019). Impaired cortical glucose metabolism and a concomitant reduction of field potential power were found in a mouse model of pyruvate dehydrogenase deficiency (Jakkamsetti et al., 2019). We also detected reduced EEG power in LPS-treated mice and increased synaptic levels of carbohydrate metabolism-related proteins. The elevated levels of these metabolic proteins may reflect a compensatory mechanism related to the disrupted energy metabolism induced by acute systemic inflammation (Kealy et al., 2020). Proinflammatory processes in response to LPS treatment trigger several signaling pathways, which results in transcription factor (TF) activation, such as FOXOs and NFκB, leading to enhanced expression of proinflammatory cytokines and pro-survival genes. FOXOs and NFκB are regulated by synaptic activity as well (O'Neill and Kaltschmidt, 1997; Hardingham and Bading, 2010) and inducible forms of NFκB are also present in synapses (Kaltschmidt et al., 1993). In the cerebral cortex of LPS-treated mice phosphorylated FOXO3a and NFκB levels were elevated (Ali et al., 2020) and we detected several significantly altered proteins that regulate these TFs. In addition, one of our previous works also revealed that LPS-induced proteomic changes of the rat thalamus and fronto-parietal cortex are related to NFκB-dependent proinflammatory processes (Györffy et al.,

2014).

We have found three members of 14-3-3 protein family that have a widespread role in cellular signaling by integrating several signaling pathways. 14-3-3 proteins bind to FOXO3a phosphorylated by Akt, and they interfere with its nuclear import that promotes cell survival (Brunet et al., 1999). The functional knockdown (FKO) of 14-3-3 proteins decreases dendritic spine density and the levels of Psd95 and NMDA-receptor subunits in mice (Foote et al., 2015; Graham et al., 2019). These effects might be regulated by the cytoskeleton since reduced levels of phospho-cofilin was found in the brain of 14-3-3 FKO mice (Foote et al., 2015). We detected elevated levels of cofilin-1, cofilin-2, 14-3-3γ, β, and ζ, which might suggest a strengthening effect on synaptic transmission in response to LPS treatment.

We have identified several significantly altered proteins related to ubiquitination that also regulate NFκB signaling, such as Ubb, Ube2v1, Ube2v2, and Ubxn1. Ubiquitination regulates proteasome-mediated protein degradation likely *via* lysine 48 (K48) of ubiquitin; however, lysine 63 (K63)-linked ubiquitination does not regulate protein degradation but modifies the activity of proteins. Ube2v1 ubiquitin ligase E2 regulates K63-linked polyubiquitination of Psd95, which affects its scaffolding abilities and facilitates synaptic strengthening (Ma et al., 2017). Ube2v1 also activates NFκB signaling *via* the inhibitor of nuclear factor kappa-B kinase (IκB) kinase in response to proinflammatory cytokines (Deng et al., 2000). However, Ubxn1 and Nsfl1c overexpression attenuated NFκB signaling in HEK293 cells upon TNF-α stimuli (Wang et al., 2015). In conclusion, we have detected increased level of an NFκB activator (Ube2v1) and decreased levels of two NFκB inhibitors (Ubxn1 and Nsfl1c), which may indicate synaptic NFκB activation upon LPS treatment. We found several connections between the altered proteins and the IL-1 signaling pathway, the most evident is Ube2v1, which is part of the canonical IL-1 signaling pathway. The Western blot analysis of PFC tissue samples likewise revealed the increased expression of IL-1R1 after LPS treatment. Also, elevated levels of Ube2v1 might promote pro-inflammatory signaling and synaptic strengthening via K63-linked polyubiquitination. Thus, the proteomic alterations of PFC synapses may affect synaptic transmission that can be linked to the LPS-induced changes of frontal EEG activity and to the neuropsychiatric consequences of acute systemic inflammation; since it has been observed in various rodent models of CNS disorders that synaptic impairments are related to behavioral and cognitive disturbances (Davari et al., 2013; Chung et al., 2015; Papaleo et al., 2016).

To conclude, the results of the present study suggest that peripherally evoked acute neuroinflammation contributes to PFC dysfunctions by different cellular and molecular mechanisms. IL-1β, a major proinflammatory cytokine seems to affect cortical excitatory/inhibitory balance *via* its different electrophysiological effects on glutamatergic and GABAergic neurons. On the other hand, PFC synapses were found to show LPS-induced proteomic changes in signaling, cytoskeletal, and metabolic processes, which may alter synaptic transmission in cortical circuits. The altered intrinsic and/or synaptic activity of PFC neurons might be associated with the observed changes of frontal EEG pattern and fronto-occipital functional connectivity. These network-level disturbances can ultimately contribute to the appearance of the well-known behavioral and cognitive symptoms of acute systemic immune challenge.

Author contribution

DM, JK, GJ, and KAK conceptualized the study and designed the experiments. DM, VT, LR, ÉC, TK, and KAK performed the experiments, and DM, VT, ÉC, and KAK analyzed the data. DM, VT, GJ, and KAK wrote the manuscript, and all co-authors reviewed and accepted its submitted version.

Funding

This study was supported by the National Research, Development and Innovation Office of Hungary (grants 2017–1.2.1-NKP-2017-00002 and FIEK_16-1-2016-0005) and National Brain Research Program NAP 3.0 of the Hungarian Academy of Sciences (NAP2022-I-3/2022) to DM, VT, LR, TK, JK, GJ and KAK; by GINOP-2.3.3-15-2016-00020 to ÉC; and by the research scholarship of Gedeon Richter Plc. Centenarial Foundation, Budapest, Hungary to DM.

Declaration of competing interest

Authors LR, TK, and GJ were employed by CRU Hungary Ltd. Authors GJ and KAK were employed by InnoScience Ltd. The remaining authors declare that they have no known competing financial interests or personal relationships that could have appeared to influence the work reported in this paper.

Data availability

Data will be made available on request.

Appendix A. Supplementary data

Supplementary data to this article can be found online at https://doi.org/10.1016/j.bbih.2023.100594.

References

Albrecht, M.A., Vaughn, C.N., Erickson, M.A., Clark, S.M., Tonelli, L.H., 2018. Time and frequency dependent changes in resting state EEG functional connectivity following lipopolysaccharide challenge in rats. PLoS One 13, 1–19. https://doi.org/10.1371/journal.pone.0206985 e0206985.

Ali, T., Rahman, S.U., Hao, Q., Li, W., Liu, Z., Ali Shah, F., Murtaza, I., Zhang, Z., Yang, X., Liu, G., Li, S., 2020. Melatonin prevents neuroinflammation and relieves depression by attenuating autophagy impairment through FOXO3a regulation. J. Pineal Res. 69, 1–18. https://doi.org/10.1111/jpi.12667 e12667.

Banks, W.A., Gray, A.M., Erickson, M.A., Salameh, T.S., Damodarasamy, M., Sheibani, N., Meabon, J.S., Wing, E.E., Morofuji, Y., Cook, D.G., Reed, M.J., 2015. Lipopolysaccharide-induced blood-brain barrier disruption: roles of cyclooxygenase, oxidative stress, neuroinflammation, and elements of the neurovascular unit. J. Neuroinflammation 12 (223), 1–15. https://doi.org/10.1186/s12974-015-0434-1.

Bastos, A.M., Schoffelen, J.M., 2016. A tutorial review of functional connectivity analysis methods and their interpretational pitfalls. Front. Syst. Neurosci. 9 (175), 1–23. https://doi.org/10.3389/fnsys.2015.00175.

Basu, A., Krady, J.K., Levison, S.W., 2004. Interleukin-1: a master regulator of neuroinflammation. J. Neurosci. Res. 78 (2), 151–156. https://doi.org/10.1002/jnr.20266.

Batista, C.R.A., Gomes, G.F., Candelario-Jalil, E., Fiebich, B.L., De Oliveira, A.C.P., 2019. Lipopolysaccharide-induced neuroinflammation as a bridge to understand neurodegeneration. Int. J. Mol. Sci. 20, 1–31. https://doi.org/10.3390/ijms20092293, 2293.

Boraschi, D., Italiani, P., Weil, S., Martin, M.U., 2018. The family of the interleukin-1 receptors. Immunol. Rev. 281 (1), 197–232. https://doi.org/10.1111/imr.12606.

Brambilla, D., Barajon, I., Bianchi, S., Opp, M.R., Imeri, L., 2010. Interleukin-1 inhibits putative cholinergic neurons in vitro and REM sleep when microinjected into the rat laterodorsal tegmental nucleus. Sleep 33, 919–929. https://doi.org/10.1093/sleep/33.7.919.

Brunet, A., Bonni, A., Zigmond, M.J., Lin, M.Z., Juo, P., Hu, L.S., Anderson, M.J., Arden, K.C., Blenis, J., Greenberg, M.E., 1999. Akt promotes cell survival by phosphorylating and inhibiting a Forkhead transcription factor. Cell 96, 857–868. https://doi.org/10.1016/s0092-8674(00)80595-4.

Buzsáki, G., Anastassiou, C.A., Koch, C., 2012. The origin of extracellular fields and currents – EEG, ECoG, LFP and spikes. Nat. Rev. Neurosci. 13, 407–420. https://doi.org/10.1038/nrn3241.

Capuron, L., Castanon, N., 2016. Role of inflammation in the development of neuropsychiatric symptom domains: evidence and mechanisms. Inflammation-associated depression: evidence, mechanisms and implications. Curr. Top. Behav. Neurosci. 31, 31–44. https://doi.org/10.1007/7854_2016_14.

Chung, W.S., Welsh, C.A., Barres, B.A., Stevens, B., 2015. Do glia drive synaptic and cognitive impairment in disease? Nat. Neurosci. 18, 1539–1545. https://doi.org/10.1038/nn.4142.

Cox, J., Mann, M., 2008. MaxQuant enables high peptide identification rates, individualized p.p.b.-range mass accuracies and proteome-wide protein quantification. Nat. Biotechnol. 26, 1367–1372. https://doi.org/10.1038/nbt.1511.

Cunningham, C., Campion, S., Lunnon, K., Murray, C.L., Woods, J.F.C., Deacon, R.M.J., Rawlins, J.N.P., Perry, V.H., 2009. Systemic inflammation induces acute behavioral

and cognitive changes and accelerates neurodegenerative disease. Biol. Psychiatr. 65, 304–312. https://doi.org/10.1016/j.biopsych.2008.07.024.
Cunningham, C., Sanderson, D.J., 2008. Malaise in the water maze: untangling the effects of LPS and IL-1β on learning and memory. Brain Behav. Immun. 22, 1117–1127. https://doi.org/10.1016/j.bbi.2008.05.007.
Dantzer, R., 2004. Cytokine-induced sickness behaviour: a neuroimmune response to activation of innate immunity. Eur. J. Pharmacol. 500, 399–411. https://doi.org/10.1016/j.ejphar.2004.07.040.
Dantzer, R., O'connor, J.C., Freund, G.G., Johnson, R.W., Kelley, K.W., 2008. From inflammation to sickness and depression: when the immune system subjugates the brain. Nat. Rev. Neurosci. 9, 46–56. https://doi.org/10.1038/nrn2297.
Davari, S., Talaei, S.A., Alaei, H., 2013. Probiotics treatment improves diabetes-induced impairment of synaptic activity and cognitive function: behavioral and electrophysiological proofs for microbiome–gut–brain axis. Neuroscience 240, 287–296. https://doi.org/10.1016/j.neuroscience.2013.02.055.
Deng, L., Wang, C., Spencer, E., Yang, L., Braun, A., You, J., Slaughter, C., Pickart, C., Chen, Z.J., 2000. Activation of the IkappaB kinase complex by TRAF6 requires a dimeric ubiquitin-conjugating enzyme complex and a unique polyubiquitin chain. Cell 103, 351–361. https://doi.org/10.1016/s0092-8674(00)00126-4.
Desson, S.E., Ferguson, A.V., 2003. Interleukin 1β modulates rat subfornical organ neurons as a result of activation of a non-selective cationic conductance. J. Physiol. 550, 113–122. https://doi.org/10.1113/jphysiol.2003.041210.
Diaz-Castro, B., Bernstein, A.M., Coppola, G., Sofroniew, M.V., Khakh, B.S., 2021. Molecular and functional properties of cortical astrocytes during peripherally induced neuroinflammation. Cell Rep. 36 (6), 1–16. https://doi.org/10.1016/j.celrep.2021.109508.
Diem, R., Hobom, M., Grötsch, P., Kramer, B., Bähr, M., 2003. Interleukin-1β protects neurons via the interleukin-1 (IL-1) receptor-mediated Akt pathway and by IL-1 receptor-independent decrease of transmembrane currents in vivo. Mol. Cell. Neurosci. 22, 487–500. https://doi.org/10.1016/s1044-7431(02)00042-8.
Dinarello, C.A., 2009. Immunological and inflammatory functions of the interleukin-1 family. Annu. Rev. Immunol. 27, 519–550. https://doi.org/10.1146/annurev.immunol.021908.132612.
DiSabato, D.J., Quan, N., Godbout, J.P., 2016. Neuroinflammation: the devil is in the details. J. Neurochem. 139, 136–153. https://doi.org/10.1111/jnc.13607.
Fan, K., Li, D., Zhang, Y., Han, C., Liang, J., Hou, C., Xiao, H., Ikenaka, K., Ma, J., 2015. The induction of neuronal death by up-regulated microglial cathepsin H in LPS-induced neuroinflammation. J. Neuroinflammation 12 (54), 1–12. https://doi.org/10.1186/s12974-015-0268-x.
Feng, X.Y., Hu, H.D., Chen, J., Long, C., Yang, L., Wang, L., 2021. Acute neuroinflammation increases excitability of prefrontal parvalbumin interneurons and their functional recruitment during novel object recognition. Brain Behav. Immun. 98, 48–58. https://doi.org/10.1016/j.bbi.2021.08.216.
Ferri, C.C., Yuill, E.A., Ferguson, A.V., 2005. Interleukin-1β depolarizes magnocellular neurons in the paraventricular nucleus of the hypothalamus through prostaglandin-mediated activation of a non selective cationic conductance. Regul. Pept. 129, 63–71. https://doi.org/10.1016/j.regpep.2005.01.004.
Fingelkurts, A.A., Fingelkurts, A.A., Rytsälä, H., Suominen, K., Isometsä, E., Kähkönen, S., 2007. Impaired functional connectivity at EEG alpha and theta frequency bands in major depression. Hum. Brain Mapp. 28, 247–261. https://doi.org/10.1002/hbm.20275.
Foote, M., Qiao, H., Graham, K., Wu, Y., Zhou, Y., 2015. Inhibition of 14-3-3 proteins leads to schizophrenia-related behavioral phenotypes and synaptic defects in mice. Biol. Psychiatr. 78, 386–395. https://doi.org/10.1016/j.biopsych.2015.02.015.
Ge, S.X., Jung, D., Yao, R., 2020. ShinyGO: a graphical gene-set enrichment tool for animals and plants. Bioinformatics 36, 2628–2629. https://doi.org/10.1093/bioinformatics/btz931.
Gennaro, L.D., Vecchio, F., Ferrara, M., Curcio, G., Rossini, P.M., Babiloni, C., 2004. Changes in fronto-posterior functional coupling at sleep onset in humans. J. Sleep Res. 13, 209–217. https://doi.org/10.1111/j.1365-2869.2004.00406.x.
Ghosal, S., Hare, B.D., Duman, R.S., 2017. Prefrontal cortex GABAergic deficits and circuit dysfunction in the pathophysiology and treatment of chronic stress and depression. Curr. Opin. Behav. Sci. 14, 1–8. https://doi.org/10.1016/j.cobeha.2016.09.012.
Ghosh, B., Green, M.V., Krogh, K.A., Thayer, S.A., 2016. Interleukin-1β activates an Src family kinase to stimulate the plasma membrane Ca2+ pump in hippocampal neurons. J. Neurophysiol. 115, 1875–1885. https://doi.org/10.1152/jn.00541.2015.
Gofton, T.E., Young, G.B., 2012. Sepsis-associated encephalopathy. Nat. Rev. Neurol. 8, 557–566. https://doi.org/10.1038/nrneurol.2012.183.
Graham, K., Zhang, J., Qiao, H., Wu, Y., Zhou, Y., 2019. Region-specific inhibition of 14-3-3 proteins induces psychomotor behaviors in mice. NPJ Schizophr 5 (1), 1–8. https://doi.org/10.1038/s41537-018-0069-1.
Guevara, M.A., Corsi-Cabrera, M., 1996. EEG coherence or EEG correlation? Int. J. Psychophysiol. 23, 145–153. https://doi.org/10.1016/s0167-8760(96)00038-4.
Gulyássy, P., Puska, G., Györffy, B.A., Todorov-Völgyi, K., Juhász, G., Drahos, L., Kékesi, K.A., 2020. Proteomic comparison of different synaptosome preparation procedures. Amino Acids 52, 1529–1543. https://doi.org/10.1007/s00726-020-02912-6.
Györffy, B., Kovács, Z., Gulyássy, P., Simor, A., Völgyi, K., Orbán, G., Baracskay, P., Szabó, Z., Janáky, T., Dobolyi, Á., Juhász, G., Czurkó, A., Kékesi, K.A., 2014. Brain protein expression changes in WAG/Rij rats, a genetic rat model of absence epilepsy after peripheral lipopolysaccharide treatment. Brain Behav. Immun. 35, 86–95. https://doi.org/10.1016/j.bbi.2013.09.001.
Hahn, C.G., Banerjee, A., MacDonald, M.L., Cho, D.S., Kamins, J., Nie, Z., Borgmann-Winter, K.E., Grosser, T., Pizzaro, A., Ciccimaro, E., Arnold, S.E., Wang, H.-Y., Blair, I.A., 2009. The post-synaptic density of human postmortem brain tissues: an experimental study paradigm for neuropsychiatric illnesses. PLoS One 4, 1–11. https://doi.org/10.1371/journal.pone.0005251 e5251.
Han, H.B., Lee, K.E., Choi, J.H., 2019. Functional dissociation of θ oscillations in the frontal and visual cortices and their long-range network during sustained attention. Eneuro 6, 1–12. https://doi.org/10.1523/ENEURO.0248-19.2019.
Hardingham, G.E., Bading, H., 2010. Synaptic versus extrasynaptic NMDA receptor signalling: implications for neurodegenerative disorders. Nat. Rev. Neurosci. 11, 682–696. https://doi.org/10.1038/nrn2911.
Hoshino, K., Hasegawa, K., Kamiya, H., Morimoto, Y., 2017. Synapse-specific effects of IL-1β on long-term potentiation in the mouse hippocampus. Biomed. Res. 38, 183–188. https://doi.org/10.2220/biomedres.38.183.
Jakkamsetti, V., Marin-Valencia, I., Ma, Q., Good, L.B., Terrill, T., Rajasekaran, K., Pichumani, K., Khemtong, C., Hooshyar, M.A., Sundarrajan, C., Patel, M.S., Bachoo, R.M., Malloy, C.R., Pascual, J.M., 2019. Brain metabolism modulates neuronal excitability in a mouse model of pyruvate dehydrogenase deficiency. Sci. Transl. Med. 11, 1–16. https://doi.org/10.1126/scitranslmed.aan0457.
Jankowsky, J.L., Derrick, B.E., Patterson, P.H., 2000. Cytokine responses to LTP induction in the rat hippocampus: a comparison of in vitro and in vivo techniques. Learn. Mem. 7, 400–412. https://doi.org/10.1101/lm.32600.
Ji, M.H., Lei, L., Gao, D.P., Tong, J.H., Wang, Y., Yang, J.J., 2020. Neural network disturbance in the medial prefrontal cortex might contribute to cognitive impairments induced by neuroinflammation. Brain Behav. Immun. 89, 133–144. https://doi.org/10.1016/j.bbi.2020.06.001.
Jiang, J., Tang, B., Wang, L., Huo, Q., Tan, S., Misrani, A., Han, Y., Li, H., Hu, H., Wang, J., Cheng, T., Tabassum, S., Chen, M., Xie, W., Long, C., Yang, L., 2022. Systemic LPS-induced microglial activation results in increased GABAergic tone: a mechanism of protection against neuroinflammation in the medial prefrontal cortex in mice. Brain Behav. Immun. 99, 53–69. https://doi.org/10.1016/j.bbi.2021.09.017.
Kaltschmidt, C., Kaltschmidt, B., Baeuerle, P.A., 1993. Brain synapses contain inducible forms of the transcription factor NF-kappa B. Mech. Dev. 43, 135–147. https://doi.org/10.1016/0925-4773(93)90031-r.
Kealy, J., Murray, C., Griffin, E.W., Lopez-Rodriguez, A.B., Healy, D., Tortorelli, L.S., Lowry, J.P., Watne, L.O., Cunningham, C., 2020. Acute inflammation alters brain energy metabolism in mice and humans: role in suppressed spontaneous activity, impaired cognition, and delirium. J. Neurosci. 40, 5681–5696. https://doi.org/10.1523/JNEUROSCI.2876-19.2020.
Kesner, R.P., Churchwell, J.C., 2011. An analysis of rat prefrontal cortex in mediating executive function. Neurobiol. Learn. Mem. 96, 417–431. https://doi.org/10.1016/j.nlm.2011.07.002.
Kunicki, C., Moioli, C.R., Pais-Vieira, M., Salles Cunha Peres, A., Morya, E., Nicolelis, M. A.L., 2019. Frequency-specific coupling in fronto-parieto-occipital cortical circuits underlie active tactile discrimination. Sci. Rep. 9, 1–14. https://doi.org/10.1038/s41598-019-41516-3.
Li, W., Ali, T., He, K., Liu, Z., Shah, F.A., Ren, Q., Liu, Y., Jiang, A., Li, S., 2021. Ibrutinib alleviates LPS-induced neuroinflammation and synaptic defects in a mouse model of depression. Brain Behav. Immun. 92, 10–24. https://doi.org/10.1016/j.bbi.2020.11.008.
Liège, S., Layé, S., Li, K.S., Moze, E., Neveu, P.J., 2000. Interleukin 1 receptor accessory protein (IL-1RAcP) is necessary for centrally mediated neuroendocrine and immune responses to IL-1β. J. Neuroimmunol. 110, 134–139. https://doi.org/10.1016/s0165-5728(00)00331-3.
Liu, X., Nemeth, D.P., McKim, D.B., Zhu, L., DiSabato, D.J., Berdysz, O., Gorantla, G., Oliver, B., Witcher, K.G., Wang, Y., Negray, C.E., Vegesna, R.S., Sheridan, J.F., Godbout, J.P., Robson, M.J., Blakely, R.D., Popovich, P.G., Bilbo, S.D., Quan, N., 2019. Cell-type-specific interleukin 1 receptor 1 signaling in the brain regulates distinct neuroimmune activities. Immunity 50 (2), 317–333. https://doi.org/10.1016/j.immuni.2018.12.012.
Ma, Q., Ruan, H., Peng, L., Zhang, M., Gack, M.U., Yao, W.D., 2017. Proteasome-independent polyubiquitin linkage regulates synapse scaffolding, efficacy, and plasticity. Proc. Natl. Acad. Sci. USA 114, E8760–E8769. https://doi.org/10.1073/pnas.1620153114.
Mamad, O., Islam, M.N., Cunningham, C., Tsanov, M., 2018. Differential response of hippocampal and prefrontal oscillations to systemic LPS application. Brain Res. 1681, 64–74. https://doi.org/10.1016/j.brainres.2017.12.036.
Martens, M., Ammar, A., Riutta, A., Waagmeester, A., Slenter, D.N., Hanspers, K., Miller, R.A., Digles, D., Lopes, E.N., Ehrhart, F., Dupuis, L.J., Winckers, L.A., Coort, S.L., Willighagen, E.L., Evelo, C.T., Pico, A.R., Kutmon, M., 2021. WikiPathways: connecting communities. Nucleic Acids Res. 49, 613–621. https://doi.org/10.1093/nar/gkaa1024.
Miller, E.K., 2000. The prefontral cortex and cognitive control. Nat. Rev. Neurosci. 1, 59–65. https://doi.org/10.1038/35036228.
Mina, F., Comim, C.M., Dominguini, D., Cassol Jr., O.J., DallIgna, D.M., Ferreira, G.K., Silva, M.C., Galant, L.S., Streck, E.L., Quevedo, J., Dal-Pizzol, F., 2014. Il1-β involvement in cognitive impairment after sepsis. Mol. Neurobiol. 49, 1069–1076. https://doi.org/10.1007/s12035-013-8581-9.
Nguyen, L., Rothwell, N.J., Pinteaux, E., Boutin, H., 2011. Contribution of interleukin-1 receptor accessory protein B to interleukin-1 actions in neuronal cells. Neurosignals 19 (4), 222–230. https://doi.org/10.1159/000330803.
Olbrich, S., Tränkner, A., Chittka, T., Hegerl, U., Schönknecht, P., 2014. Functional connectivity in major depression: increased phase synchronization between frontal cortical EEG-source estimates. Psychiatry Res. Neuroimaging. 222, 91–99. https://doi.org/10.1016/j.pscychresns.2014.02.010.

O'Neill, L.A., Kaltschmidt, C., 1997. NF-kappa B: a crucial transcription factor for glial and neuronal cell function. Trends Neurosci. 20, 252–258. https://doi.org/10.1016/s0166-2236(96)01035-1.

Papaleo, F., Yang, F., Paterson, C., Palumbo, S., Carr, G.V., Wang, Y., Floyd, K., Huang, W., Thomas, C.J., Chen, J., Weinberger, D.R., Law, A.J., 2016. Behavioral, neurophysiological, and synaptic impairment in a transgenic neuregulin1 (NRG1-IV) murine schizophrenia model. J. Neurosci. 36, 4859–4875. https://doi.org/10.1523/JNEUROSCI.4632-15.2016.

Paxinos, G., Franklin, K.B.J., 2001. The Mouse Brain in Stereotaxic Coordinates, second ed. Deluxe) By Academic Press, New York, ISBN 0-12-547637-X.

Phillips, G.R., Huang, J.K., Wang, Y., Tanaka, H., Shapiro, L., Zhang, W., Shan, W.S., Arndt, K., Frank, M., Gordon, R.E., Gawinowicz, M.A., Zhao, Y., Colman, D.R., 2001. The presynaptic particle web: ultrastructure, composition, dissolution, and reconstitution. Neuron 32, 63–77. https://doi.org/10.1016/s0896-6273(01)00450-0.

Pinteaux, E., Trotter, P., Simi, A., 2009. Cell-specific and concentration-dependent actions of interleukin-1 in acute brain inflammation. Cytokine 45 (1), 1–7. https://doi.org/10.1016/j.cyto.2008.10.008.

Puris, E., Kouřil, Š., Najdekr, L., Auriola, S., Loppi, S., Korhonen, P., Gómez-Budia, M., Fricker, G., Kanninen, K.M., Malm, T., Friedecký, D., Gynther, M., 2022. Metabolomic, lipidomic and proteomic characterisation of lipopolysaccharide-induced inflammation mouse model. Neuroscience 496, 165–178. https://doi.org/10.1016/j.neuroscience.2022.05.030.

Ravasz, L., Kékesi, K.A., Mittli, D., Todorov, M.I., Borhegyi, Z., Ercsey-Ravasz, M., Tyukodi, B., Wang, J., Bártfai, T., Eberwine, J., Juhász, G., 2021. Cell surface protein mRNAs show differential transcription in pyramidal and fast-spiking cells as revealed by single-cell sequencing. Cerebr. Cortex 31, 731–745. https://doi.org/10.1093/cercor/bhaa195.

Rizzo, F.R., Musella, A., De Vito, F., Fresegna, D., Bullitta, S., Vanni, V., Guadalupi, L., Bassi, M.S., Buttari, F., Mandolesi, G., Centonze, D., Gentile, A., 2018. Tumor necrosis factor and interleukin-1β modulate synaptic plasticity during neuroinflammation. Neural Plast. 1–12. https://doi.org/10.1155/2018/8430123, 2018.

Samios, V.N., Inoue, T., 2014. Interleukin-1β and interleukin-6 affect electrophysiological properties of thalamic relay cells. Neurosci. Res. 87, 16–25. https://doi.org/10.1016/j.neures.2014.06.011.

Sauseng, P., Klimesch, W., Doppelmayr, M., Pecherstorfer, T., Freunberger, R., Hanslmayr, S., 2005. EEG alpha synchronization and functional coupling during top-down processing in a working memory task. Hum. Brain Mapp. 26, 148–155. https://doi.org/10.1002/hbm.20150.

Schwarz, J.M., Bilbo, S.D., 2011. LPS elicits a much larger and broader inflammatory response than Escherichia coli infection within the hippocampus of neonatal rats. Neurosci. Lett. 497 (2), 110–115. https://doi.org/10.1016/j.neulet.2011.04.042.

Shannon, P., Markiel, A., Ozier, O., Baliga, N.S., Wang, J.T., Ramage, D., Amin, N., Schwikowski, B., Ideker, T., 2003. Cytoscape: a software environment for integrated models of biomolecular interaction networks. Genome Res. 13, 2498–2504. https://doi.org/10.1101/gr.1239303.

Sheppard, O., Coleman, M.P., Durrant, C.S., 2019. Lipopolysaccharide-induced neuroinflammation induces presynaptic disruption through a direct action on brain tissue involving microglia-derived interleukin 1 beta. J. Neuroinflammation 16, 1–13. https://doi.org/10.1186/s12974-019-1490-8.

Siegel, M., Buschman, T.J., Miller, E.K., 2015. Cortical information flow during flexible sensorimotor decisions. Science 348, 1352–1355. https://doi.org/10.1126/science.aab0551.

Silfverhuth, M.J., Hintsala, H., Kortelainen, J., Seppänen, T., 2012. Experimental comparison of connectivity measures with simulated EEG signals. Med. Biol. Eng. Comput. 50, 683–688. https://doi.org/10.1007/s11517-012-0911-y.

Skaper, S.D., Facci, L., Zusso, M., Giusti, P., 2018. An inflammation-centric view of neurological disease: beyond the neuron. Front. Cell. Neurosci. 12 (72), 1–26. https://doi.org/10.3389/fncel.2018.00072.

Skelly, D.T., Griffin, É.W., Murray, C.L., Harney, S., O'Boyle, C., Hennessy, E., Dansereau, M.-A., Nazmi, A., Tortorelli, L., Rawlins, J.N., Bannerman, D.M., Cunningham, C., 2019. Correction: acute transient cognitive dysfunction and acute brain injury induced by systemic inflammation occur by dissociable IL-1-dependent mechanisms. Mol. Psychiatr. 24, 1566. https://doi.org/10.1038/s41380-019-0403-7, 1566.

Szegő, É.M., Janáky, T., Szabó, Z., Csorba, A., Kompagne, H., Müller, G., Lévay, G., Simor, A., Juhász, G., Kékesi, K.A., 2010. A mouse model of anxiety molecularly characterized by altered protein networks in the brain proteome. Eur. Neuropsychopharmacol 20, 96–111. https://doi.org/10.1016/j.euroneuro.2009.11.003.

Szklarczyk, D., Gable, A.L., Nastou, K.C., Lyon, D., Kirsch, R., Pyysalo, S., Doncheva, N. T., Legeay, M., Fang, T., Bork, P., Jensen, L.J., von Mering, C., 2021. The STRING database in 2021: customizable protein–protein networks, and functional characterization of user-uploaded gene/measurement sets. Nucleic Acids Res. 49, 605–612. https://doi.org/10.1093/nar/gkaa1074.

Tabarean, I.V., Korn, H., Bartfai, T., 2006. Interleukin-1β induces hyperpolarization and modulates synaptic inhibition in preoptic and anterior hypothalamic neurons. Neuroscience 141, 1685–1695. https://doi.org/10.1016/j.neuroscience.2006.05.007.

Tukacs, V., Mittli, D., Györffy, B.A., Hunyady-Gulyás, É., Hlatky, D., Tóth, V., Ravasz, L., Medzihradszky, F.K., Nyitrai, G., Czurkó, A., Juhász, G., Kardos, J., Kékesi, K.A., 2020. Chronic stepwise cerebral hypoperfusion differentially induces synaptic proteome changes in the frontal cortex, occipital cortex, and hippocampus in rats. Sci. Rep. 10, 1–12. https://doi.org/10.1038/s41598-020-72868-w.

Vijayan, V., Pradhan, P., Braud, L., Fuchs, H.R., Gueler, F., Motterlini, R., Foresti, R., Immenschuh, S., 2019. Human and murine macrophages exhibit differential metabolic responses to lipopolysaccharide - a divergent role for glycolysis. Redox Biol. 22, 1–9. https://doi.org/10.1016/j.redox.2019.101147, 101147.

Viviani, B., Bartesaghi, S., Gardoni, F., Vezzani, A., Behrens, M.M., Bartfai, T., Binaglia, M., Corsini, E., Di Luca, M., Galli, C.L., Marinovich, M., 2003. Interleukin-1β enhances NMDA receptor-mediated intracellular calcium increase through activation of the Src family of kinases. J. Neurosci. 23, 8692–8700. https://doi.org/10.1523/JNEUROSCI.23-25-08692.2003.

Wang, H.L., Sun, Y.X., Liu, X., Wang, H., Ma, Y.N., Su, Y.A., Li, J.T., Si, T.M., 2019. Adolescent stress increases depression-like behaviors and alters the excitatory-inhibitory balance in aged mice. Chin. Med. J. 132, 1689–1699. https://doi.org/10.1097/CM9.0000000000000313.

Wang, Y.B., Tan, B., Mu, R., Chang, Y., Wu, M., Tu, H.Q., Zhang, Y.C., Guo, S.S., Qin, X. H., Li, T., Li, W.H., Li, A.L., Zhang, X.M., Li, H.Y., 2015. Ubiquitin-associated domain-containing ubiquitin regulatory X (UBX) protein UBXN1 is a negative regulator of nuclear factor κB (NF-κB) signaling. J. Biol. Chem. 290, 10395–10405. https://doi.org/10.1074/jbc.M114.631689.

Wang, Z., Li, W., Chen, J., Shi, H., Zhao, M., You, H., Rao, C., Zhan, Y., Yang, Y., Xie, P., 2016. Proteomic analysis reveals energy metabolic dysfunction and neurogenesis in the prefrontal cortex of a lipopolysaccharide-induced mouse model of depression. Mol. Med. Rep. 13, 1813–1820. https://doi.org/10.3892/mmr.2015.4741.

Woodburn, S.C., Bollinger, J.L., Wohleb, E.S., 2021. The semantics of microglia activation: neuroinflammation, homeostasis, and stress. J. Neuroinflammation 18 (258), 1–16. https://doi.org/10.1186/s12974-021-02309-6.

Xin, Y.R., Jiang, J.X., Hu, Y., Pan, J.P., Mi, X.N., Gao, Q., Xiao, F., Zhang, W., Luo, H.M., 2019. The immune system drives synapse loss during lipopolysaccharide-induced learning and memory impairment in mice. Front. Aging Neurosci. 11 (279), 1–9. https://doi.org/10.3389/fnagi.2019.00279.

Yan, Z., Rein, B., 2021. Mechanisms of synaptic transmission dysregulation in the prefrontal cortex: pathophysiological implications. Mol. Psychiatr. 27, 445–465. https://doi.org/10.1038/s41380-021-01092-3.

Zhao, J., Bi, W., Xiao, S., Lan, X., Cheng, X., Zhang, J., Lu, D., Wei, W., Wang, Y., Li, H., Fu, Y., Zhu, L., 2019. Neuroinflammation induced by lipopolysaccharide causes cognitive impairment in mice. Sci. Rep. 9, 1–12. https://doi.org/10.1038/s41598-019-42286-8, 5790.

Zhao, Z., Wang, Y., Zhou, R., Li, Y., Gao, Y., Tu, D., Wilson, B., Song, S., Feng, J., Hong, J.-S., Yakel, J.L., 2020. A novel role of NLRP3-generated IL-1β in the acute-chronic transition of peripheral lipopolysaccharide-elicited neuroinflammation: implications for sepsis-associated neurodegeneration. J. Neuroinflammation 17 (64), 1–19. https://doi.org/10.1186/s12974-020-1728-5.

Zheng, C., Zhang, T., 2015. Synaptic plasticity-related neural oscillations on hippocampus–prefrontal cortex pathway in depression. Neuroscience 292, 170–180. https://doi.org/10.1016/j.neuroscience.2015.01.071.

Zhou, C., Qi, C., Zhao, J., Wang, F., Zhang, W., Li, C., Jing, J., Kang, X., Chai, Z., 2011. Interleukin-1β inhibits voltage-gated sodium currents in a time-and dose-dependent manner in cortical neurons. Neurochem. Res. 36, 1116–1123. https://doi.org/10.1007/s11064-011-0456-8.

Zhou, Y., Zhou, B., Pache, L., Chang, M., Khodabakhshi, A.H., Tanaseichuk, O., Benner, C., Chanda, S.K., 2019. Metascape provides a biologist-oriented resource for the analysis of systems-level datasets. Nat. Commun. 10, 1–10. https://doi.org/10.1038/s41467-019-09234-6.